Typhoid toxin exhausts the RPA response to DNA replication stress driving senescence and *Salmonella* infection

Angela EM Ibler[1,2], Mohamed ElGhazaly[1], Kathryn L Naylor[1], Natalia A Bulgakova[1], Sherif El Khamisy[3,4], Daniel Humphreys[1,*]

[1]Department of Biomedical Science. University of Sheffield, United Kingdom, S10 2TN

[2]Department of Pathology, Tennis Court Road, University of Cambridge, United Kingdom, CB2 1QP

[3]The Healthy Life Span Institute, Department of Molecular Biology and Biotechnology. University of Sheffield, United Kingdom, S10 2TN

[4]Center of Genomics, Zewail City of Science and Technology, Giza, Egypt

[*]Correspondence: d.humphreys@sheffield.ac.uk

Abstract

Salmonella Typhi activates the host DNA damage response through the typhoid toxin, facilitating typhoid symptoms and chronic infections. Here we reveal a non-canonical DNA damage response, which we call RING (response induced by a genotoxin), characterized by accumulation of phosphorylated histone H2AX (γH2AX) at the nuclear periphery. RING is the result of persistent DNA damage mediated by toxin nuclease activity and is characterized by hyperphosphorylation of RPA, a sensor of single-stranded DNA (ssDNA) and DNA replication stress. The toxin overloads the RPA pathway with ssDNA substrate, causing RPA exhaustion and senescence. Senescence is also induced by canonical γH2AX foci revealing distinct mechanisms. Senescence is transmitted to non-intoxicated bystander cells by an unidentified senescence-associated secreted factor that enhances *Salmonella* infections. Thus, our work uncovers a mechanism by which genotoxic *Salmonellae* exhaust the RPA response by inducing ssDNA formation, driving host cell senescence and facilitating infection.

Introduction

Damage to our genomes, arising endogenously during DNA replication, or exogenously from genotoxins, often generates DNA breaks causing mutations and chromosomal aberrations, which underlie diseases[1]. To counteract DNA damage and its transmission during cell division, cells detect DNA damage through the DNA damage response (DDR) that orchestrates repair and cell fate decisions including survival, apoptosis and senescence[1-4].

Master regulators of the DDR are the kinases ATM (ataxia-telangiectasia mutated) and ATR (ATM and rad3-related) that phosphorylate diverse substrates to regulate DNA repair and the cell-cycle[1]. In a canonical DDR, ATM responds to DNA double strand breaks (DSBs) while ATR senses stress exerted during DNA replication but interconnected functions are described[5]. Replication stress is predominantly caused by damaged DNA replication forks, an aberrant structure yielding single-stranded DNA (ssDNA) that recruits the ssDNA-binding protein complex RPA[6] (replication protein A). RPA coats and protects ssDNA while recruiting and activating ATR[7] to further counteract DNA damage arising from replication stress[8]. The ATR pathway pauses the cell cycle, halts firing of DNA replication at new sites and stabilises forks for repair. This is key as persistent replication stress converts forks into DSBs, the most lethal form of damage that is counteracted by the ATM pathway[1, 5]. Uniting the functions of ATM and ATR is phosphorylation of their effector, histone H2AX at S139 (γH2AX)[9, 10], which represents a signature of DDRs[1, 5]. γH2AX recruits and retains DDR proteins at sites of DNA damage to coordinate repair and cell fate[1-4].

Given the importance of the DDR in coordinating diverse cellular processes, it is perhaps not surprising that pathogenic bacteria have evolved sophisticated ways to manipulate the host DDR to execute virulence strategies and establish infections[11]. This is exemplified by genotoxic strains of *Salmonella*[12-16], particularly the human-adapted intracellular pathogen *Salmonella* Typhi that underlies 21 million infections and 200,000 deaths each year[17]. The problem is exacerbated by chronically infected carriers, like the infamous typhoid Mary, who do not exhibit typhoid symptoms but retain *S.*Typhi in the population and transmit the pathogen through contaminated faeces[17]. The mechanisms by which the two disease manifestations, typhoid fever and chronic carriage, are mediated remain unclear. Experiments in animal models showed that the mortal symptoms of typhoid and chronic carriage were facilitated through a virulence factor called the typhoid toxin[13, 14]. The toxin enters human cells where it is thought to cause DNA damage through putative nuclease activity[12, 18].

The typhoid toxin is unique, comprising a pentameric PltB subunit linked to PltA, which is bound to the genotoxic DNase1-like subunit CdtB[12, 13], a subunit found in related cytolethal distending toxins (CDTs). Canonical CDTs possess DNA nickase activity implicated in the direct formation of DSBs and ssDNA breaks (SSBs)[19-21] that activate ATM/ATR pathways and induce G1 and G2 cell-cycle arrest[22-25]. Toxigenic *Salmonellae* invade human host cells where they reside within *Salmonella*-containing vacuoles and express the typhoid toxin that is exocytosed into the extracellular milieu[12, 26, 27]. Once deployed, the PltB subunit binds bystander cell surface receptors to trigger uptake after which the CdtB traffics to the nucleus and induces DDRs marked by γH2AX, cell cycle arrest and cellular distension[12, 18, 28]. The typhoid toxin has been shown to induce fever and mortality in animal models[13], and facilitate systemic infections and chronic *Salmonella* carriage[14, 16]. Understanding the toxin is especially important as it is also encoded by related *Salmonella* serovars including *S.*Paratyphi and *S.*Javiana that cause disease in humans and food-chain animals worldwide[15, 29].

Despite its importance, the cellular DDR responses to the typhoid toxin are unclear and the mechanisms by which it promotes infection are not understood. Here, we report a non-canonical DDR to ssDNA induction by the typhoid toxin that drives senescence and infection.

Results

A non-canonical DDR induced by the typhoid toxin.

To study host cell responses to the typhoid toxin, we purified recombinant holotoxin (henceforth toxin) from *Escherichia coli* and confirmed the presence of epitope-tagged $PltB^{HIS}$, $PltA^{Myc}$, and $CdtB^{FLAG}$ by SDS-PAGE and immunoblotting (**Fig 1A**, **B, Supplementary Figure 1A, 1B**). The typhoid toxin is known to trigger cell cycle arrest and the DDR in mammalian cells[12, 18, 28]. Thus, asynchronous human HT1080 cells were intoxicated for 2h followed by a chase period of 24h. Cell cycle progression was examined using the DNA-binding dye propidium iodide and flow cytometry to determine DNA content (**Fig 1C, Supplementary Fig 1C, 1D**). Untreated cells progressing through the cell cycle were predominantly observed in G1 (~75%) with ~13% in S-phase and ~17% in G2. In contrast, intoxication with wild-type toxin ($toxin^{WT}$) triggered cell-cycle arrest (**Fig 1C:** G1, ~30%; G2/M, ~60%; S ~10%, **Supplementary Fig 1E**). This response was driven by the catalytic activity of CdtB as mutation of H160 ($toxin^{HQ}$) had no effect on cell cycle progression, which was equivalent to control (**Fig 1C, Supplementary Fig 1E**).

DDR activation is marked by phosphorylation of H2AX at S139 (γH2AX)[9, 10]. Immunofluorescence microscopy showed that $toxin^{WT}$ triggered formation of γH2AX, which accumulated in distinct foci (**Fig 1D**: white arrows). This was expected as a classical DNA damage checkpoint has been previously observed for the typhoid toxin and related CDTs[12, 18, 25, 28, 30, 31]. To our surprise, we found that γH2AX was not observed in foci in a significant proportion of intoxicated host cells (**Fig 1D**). Instead, γH2AX was found enriched in rings circling the edge of the nuclear periphery (blue arrows), which was also observed at high resolution by Airyscan confocal microscopy (**Fig 1E**). Both γH2AX phenotypes were mutually exclusive as foci were never observed in cells with rings (exemplified by the arrows in **Fig 1D**). Rings of γH2AX were neither observed in control cells nor in cells treated with $toxin^{HQ}$ (**Fig 1D**).

To examine the γH2AX phenotype more closely, we established an image-based 'RING Tracking' method, which automated segmentation of γH2AX phenotypes and quantified γH2AX rings in cell populations (**Supplementary Fig 2**). Classical γH2AX foci were present in ~15% of intoxicated cells while non-canonical γH2AX rings were found in ~50% (**Fig 1F**). Rings were observed in all cell lines tested, varying between ~25% to ~55% of cells (**Supplementary Fig 3A**). This included mouse embryonic fibroblasts (MEFs) imaged by high-resolution structured illumination microscopy (**Supplementary Fig 3B**). Increasing the

dose 10-fold from 5ng/ml to 50ng/ml had no additive effect on RING formation (**Fig 1G**), which was maximal in 50% of HT1080s suggesting an unidentified limiting factor. In contrast, decreasing the toxin dose 10-fold to 0.5ng/ml resulted in loss of RING formation, which could be significantly increased by extending the toxin^{WT} incubation from 2h to 8h. Thus, rings of γH2AX are induced in a dose-dependent manner.

γH2AX localisation at the nuclear periphery has been reported as a caspase-dependent marker of early apoptosis[32, 33]. However, in contrast to the known apoptosis inducer staurosporine, neither toxin^{WT} nor toxin^{HQ} induced significant apoptotic cell death, activation of the caspase cascade or cleavage of the caspase substrate PARP1 (**Supplementary Fig 4A, 4B**). Moreover, while the pan-caspase inhibitor ZVAD-OMe-FMK blocked caspase activation (**Supplementary Fig 4C**), it had no effect on toxin-induced γH2AX rings (**Supplementary Fig 4D**) confirming their independence from apoptosis.

γH2AX acts as a hub by recruiting DNA repair proteins such as 53BP1[1-3] (p53-binding protein 1). Indeed, 53BP1 was either diffusely localised across the nucleus or below detection in untreated controls (**Fig 1D, Supplementary Fig 5A**) but in intoxicated cells (toxin^{WT}), the proportion of cells with 53BP1 foci significantly increased (**Fig 1D, 1H**). Relative to untreated controls, toxin^{HQ} induced a modest but reproducible increase in γH2AX (**Fig 1D**) and 53BP1 foci (**Fig 1D, 1H**), which was likely due to LPS contamination that binds His-tagged proteins and activates DDRs[34-36]. The γH2AX foci in toxin^{WT}-treated host cells invariably co-localised with 53BP1 (white arrows) but not in untreated controls (**Fig 1D**). In toxin^{WT}-treated cells displaying γH2AX rings however, no 53BP1 co-localisation was apparent (blue arrows) showing that 53BP1 had uncoupled from the γH2AX pathway (**Fig 1D, 1I**). The uncoupling of γH2AX from the canonical 53BP1 pathway and its localisation in rings at the nuclear periphery mark the discovery of a non-canonical host cell γH2AX **r**esponse **in**duced by a **g**enotoxin (henceforth RING).

RINGs are triggered by *Salmonella* and related genotoxins. We next examined γH2AX RINGs during bacterial infection. *Salmonella* enterica serovars Typhi, Paratyphi, Javiana and Montevideo are known to target host cells with the typhoid toxin[12, 28, 37]. Intracellular toxigenic *Salmonella* secrete the typhoid toxin into the extracellular environment from where the toxin intoxicates bystander host cells[12, 16]. When we infected HT1080 cells with toxigenic strains of *S.*Typhi or *S.*Javiana, DDRs were observed as γH2AX foci at 24h post infection (white arrows in **Fig 1J**). Remarkably, infection also induced RINGs (blue arrows in **Fig 1J**), which increased from ~25% at 24h to ~50% by 48h and were not induced by toxin-deficient strains (Δ*cdtB*) (**Fig 1J, Supplementary Fig 5B, 5C**).

The typhoid toxin is a unique chimera of CdtB, the toxigenic subunit of CDTs, and pertussis toxin[12, 13]. CDTs comprise CdtA, CdtC and CdtB that are encoded by diverse bacterial pathogens[25]. Remarkably, like the typhoid toxin, purified CDT from pathogenic *E.coli* (EcCDT) also induced both DNA damage foci (white arrow), as previously reported[25], and RINGs in ~30% of intoxicated host cells at 24h (blue arrows) (**Fig 1K**). Thus, RING formation is a phenomenon conserved amongst canonical and non-canonical CDTs.

RINGs are triggered in S-phase of the cell cycle.

We next addressed the mechanisms by which γH2AX RINGs develop. 53BP1 localises to pre-replicative chromatin and is negatively regulated in S-phase[38], which may explain the exclusion of 53BP1 from RINGs (**Fig 1D, 1I**). Our interest in S-phase was furthered by the specific localisation of γH2AX in RINGs that was reminiscent of heterochromatin, which is refractory to γH2AX production until late S-phase when heterochromatin is decompacted for replication[1, 39, 40]. Indeed, γH2AX in RINGs co-localised with heterochromatin marked by histone-3 lysine-9 methylation (**Supplementary Fig 5D, 5E**: H3K9me3). Thus, we next examined the significance of S-phase in RING formation.

We arrested cells in G1 by serum starvation to block entry into S-phase (**Supplementary Fig 6A**) before assaying RING formation (**Fig 2**). In the presence of serum (+serum), RINGs were observed in ~20% of cells at 6h and ~50% by 48h (**Fig 2A**). When cells were prevented entry into S-phase (- serum), RING formation was completely abolished and the DNA damage phenotype was limited to γH2AX foci (**Fig 2A, 2B**). When intoxicated serum-starved cells were permitted entry into S-phase by addition of serum at 24h (released), we observed RINGs in ~40% of cells by 48h (**Fig 2A, 2C, 2D**) showing a requirement for S-phase in RING formation at heterochromatin.

To address whether RINGs were generated in S-phase, we used fluorescently labelled nucleotide analogues BrdU and EdU to assay DNA synthesis during RING formation. $Toxin^{WT}$ inhibited global BrdU incorporation confirming a reduction in DNA synthesis (**Supplementary Fig 6B, 6C**). 2h intoxication before 24h incubation with EdU demonstrated DNA replication in RING cells by 24h (**Fig 2E, 2F**). Interestingly, γH2AX foci cells contained no EdU demonstrating G1 arrest (**Fig 2E**) that were observed by flow cytometry (**Fig 1C, Supplementary Fig 1E**). This further confirms that γH2AX/53BP1 foci in **Fig 1D** mark 53BP1-labelled damage on pre-replicative chromatin[38], which peaked in serum-starved cells (**Supplementary Fig 6D**). RINGs were maximal at 48h (**Fig 2A, Supplementary Fig 5B**), thus, we reasoned that a short 1h pulse with EdU at 24h when RINGs were reaching maximum would also reveal damage during S-phase, which was likely still in progress in a

sub-population of cells. Indeed, a significant population of RING cells with newly synthesised DNA were observed (**Fig 2F**: 1h) establishing that RINGs signify damage in S-phase.

RINGs are dependent upon regulator of replication stress ATR.

We hypothesised that RINGs signal activation of ATR that counteracts DNA replication stress by phosphorylating diverse substrates including H2AX and CHK1[1, 5]. To resolve whether ATR determines the specific localisation of γH2AX at RINGs, we intoxicated cells in the presence of ATR (iATR) and ATM (iATM) inhibitors (**Figs 2G, 2H, Supplementary Fig 6E, 6F**). Remarkably, RINGs were driven through ATR (**Fig 2G:** blue arrows, **2H**), while γH2AX foci that mark G1-arrested cells required ATM (**Fig 2G:** white arrows**, 2H**). Moreover, activated ATR and ATM were observed in intoxicated cells (**Fig 3A, Supplementary Fig 6E, 6F**). Consistent with ATR-driven RING formation, phosphorylation of CHK1 (pCHK1) and γH2AX were induced in RING permissive conditions (**Fig 2D:** +serum, **Supplementary Fig 6G**). In the presence of serum, bulk analysis by immunoblotting consistently revealed maximal γH2AX signal (**Fig 2D:** +serum), which was consistent with fluorescent images (**Fig 2B**). This likely reflects the presence of both γH2AX foci and RINGs in populations with serum whereas serum-starved cells only have foci and thus show less γH2AX signal (**Fig 2B, 2D**). Indeed, both CHK1 activation and γH2AX signal were inhibited by serum-starvation and restored in released cells (**Fig 2D**). Similarly, both RINGs and pCHK1/γH2AX were apparent in replicating THP1 monocyte cells (-PMA) but were absent in terminally differentiated non-replicating THP1 macrophage cells (+PMA) (**Supplementary Fig 6H, 6I**). Taken together, these findings show that the typhoid toxin triggers DNA damage foci in G1 through ATM but cell entry into S-phase induces ATR-dependent RING formation in response to replication stress.

ssDNA sensor RPA accumulates on the chromatin of RING cells.

The heterotrimeric complex RPA (Replication Protein A70, 32 and 14) senses replication stress by coating ssDNA at damaged replication forks where it activates ATR[5, 7]. If replication stress is not resolved then damaged forks can collapse leading to DSBs. Damaged replication forks are marked by ATR-mediated hyper-phosphorylation of ssDNA-bound RPA2 on multiple sites including T21 and S33[41, 42], which facilitate recruitment of repair factors to stalled forks[43].

To study the significance of RPA in RING formation, we examined phosphorylation of ssDNA-bound RPA in intoxicated cells (**Fig 3A, Supplementary Fig 7**). Consistent with ATR activation at damaged forks, RING formation was marked by hyper-phosphorylation of RPA32 that migrated more slowly than the RPA32 in untreated or toxin^{HQ}-treated cells. Indeed, only toxin^{WT} triggered phosphorylation of S33 (pRPA32). RPA phosphorylation was

first observed at 6h and continued to accumulate over 24h, which was also found for ATR activation and its targets CHK1 and H2AX (**Fig 3A**). Finally, when we examined RPA loading onto chromatin by cell extraction and fluorescence microscopy, RPA32 pT21 (pRPA) foci were observed confirming that RING-positive cells contained damaged replication forks (toxin^{WT}), which were not found in the control (toxin^{HQ}) (**Fig 3B, 3C**). Strikingly, RPA foci were restricted to those with RINGs (blue arrows; ~65% pRPA positive) and not γH2AX foci (white arrows; ~3% pRPA positive) (**Fig 3B, 3C**).

Typhoid toxin triggers RINGs by causing RPA exhaustion.

RPA protects ssDNA from breakage[5, 42, 44] and is phosphorylated in response to accumulating ssDNA[5, 7]. The typhoid toxin possesses endonuclease activity (**Supplementary Fig 8A**) which, in related CDTs, is known to introduce ssDNA breaks[19, 21]. Physical DNA breaks were also observed in intoxicated cells (**Supplementary Fig 8B, 8C**), which is consistent with RING formation by EcCDT (**Fig 1K**) that is known to mimic DNA damaging agents by causing DNA breaks[23]. Thus, phosphorylated RPA likely signified accumulating ssDNA in response to toxin nuclease activity. Consequently, we predicted that depleting the pool of RPA by siRNA transfection (siRPA) would sensitise cells to the typhoid toxin and RING formation (**Fig 3D-G, Supplementary Fig 8D**). To our surprise, RPA knockdown alone was sufficient to cause RINGs (**Fig 3F:** white arrow), which was co-incident with increased γH2AX (**Fig 3D**) and G2 cell-cycle arrest (**Fig 3E**) establishing that siRPA phenocopied the typhoid toxin (**Fig 3G**). Like toxin-induced RING formation (**Fig 2G, 2H**), ATR was critical to siRPA-induced RINGs, which were impeded by siATR transfection (**Supplementary Fig 8E**).

RPA binds ssDNA in stoichiometric fashion and is considered rate limiting for protecting ssDNA at replication forks[5, 42]. Thus, we hypothesised that insufficient RPA available to bind ssDNA was the common denominator for RING-induction, which was driven by loss of RPA itself (i.e. siRPA) or by unregulated supply of ssDNA (i.e. via toxin nuclease activity). Indeed, when RPA-knockdown cells were treated with toxin, there was no additive effect in RINGs (**Fig 3G:** red circles). Moreover, low concentrations of siRPA (**Fig 3G**: 5nM) and tox^{WT} (**Fig 1F**: 0.05ng/ml) that were normally insufficient for RING formation, synergised to induce RINGs (**Supplementary Fig 8F**) further establishing that RINGs are formed via RPA exhaustion.

We hypothesised that increasing the cellular pool of RPA would defend cells against the toxin and RING formation. To test this possibility, we intoxicated U2OS cells engineered to stably express additional RPA complex[44], which we confirmed by immunoblotting (**Fig 3H**, **Supplementary Fig 9**) before imaging and RING Tracking (**Fig 3I, 3J**). Intoxicated U2OS

control cells (ctrl) formed RINGs but by extending the dynamic range of ssDNA protection in 'super RPA cells', RING formation was reduced by ~50% (**Fig 3I**), which is exemplified in **Fig 3J**. No RINGs were observed with toxin^{HQ}. A similar trend was also observed in bulk analysis by immunoblotting where toxin-induction of γH2AX was markedly reduced in super RPA cells, approximately ~50% (**Fig 3H, Supplementary Figure 9D**), which mirrored the reduction in RINGs (**Fig 3I**). This was likely due to a delay in RPA exhaustion as indicated by the abundance of non-phosphorylated RPA32 (blue arrow) in the population of super RPA cells relative to toxin^{WT}-treated control cells where RPA was predominantly hyper-phosphorylated (red arrow) (**Fig 3H**). Indeed, the enzymatic activity of toxin^{WT} was still able to overcome super RPA cells, which generated RINGs and failed to resume proliferation following intoxication (**Fig 3I**, **Supplementary Fig 10A, 10B**). Together, these findings show that RING formation is a consequence of RPA exhaustion.

Typhoid toxin exhausts RPA by oversupply of ssDNA substrate.

The findings support the view that RINGs were induced by an imbalance between RPA and ssDNA substrate, which caused RPA exhaustion. To study RPA exhaustion more directly, we developed an assay that exploited ssDNA protection by RPA (depicted in **Supplementary Fig 10C**). In the RPA protection assay, we predicted that exposed ssDNA would act as a DNA template for polymerisation of BrdU-labelled DNA by exogenous DNA polymerase, which would be sterically hindered by coats of RPA loaded on ssDNA. Thus, DNA polymerase would preferentially access unprotected tracks of ssDNA in RPA-exhausted cells. The toxin^{WT} induced significantly more ssDNA-derived BrdU foci (ssDNA^{BrdU}) than control toxin^{HQ} (**Fig 4A, 4B**). Aphidicolin (APH), an inhibitor of DNA replication that generates extended tracks of ssDNA by inhibition of DNA polymerases[45], also induced ssDNA^{BrdU} (**Fig 4B, Supplementary Fig 10D**) supporting the view that the toxin generates ssDNA. Moreover, RPA foci in toxin^{HQ}-treated cells lacked ssDNA^{BrdU} indicating RPA protection of ssDNA (**Fig 4A**, magnified inset) while toxin^{WT} generated ssDNA^{BrdU} foci that were either partially protected (white arrow indicating RPA co-localisation) or completely unprotected by RPA (blue arrow). Similarly, unprotected ssDNA^{BrdU} foci were also found in APH-treated cells (**Supplementary Fig 10D**). These findings provide evidence that the toxin exhausts RPA by oversupply of ssDNA substrate.

We next sought to investigate the order of events leading to RPA exhaustion that underpinned RINGs. It was possible that toxin^{WT} nuclease activity (**Supplementary Fig 8A-C**) caused an initial burst of DNA damage independently of DNA replication that exhausted RPA. We observed toxin-induced RPA foci in non-replicating G1-arrested cells lacking EdU-labelled DNA (**Supplementary Fig 10E:** white arrows). Moreover, the toxin^{WT} triggered modest but significant RPA-loading onto chromatin in serum-starved cells suggesting

damage independently of DNA replication (**Fig 4C**). We hypothesised that DNA breaks generated in G1 together with toxin attack at replication forks would increase the load of ssDNA thereby causing RPA exhaustion in S-phase, which triggers DNA damage manifesting as RINGs. Indeed, while RPA foci were observed in ~7% of intoxicated serum-starved cells, this increased to ~60% in the presence of serum in a toxin^{WT}-dependent manner (**Fig 4C, 4D**) showing increased RPA sequestration. Moreover, like RINGs in **Fig 2E**, RPA foci accumulated in intoxicated cells that incorporated EdU (**Supplementary Fig 10E**: blue arrows) further establishing a direct relationship between DNA replication and toxin-induced ssDNA. We predicted that ssDNA accumulation via aphidicolin treatment would phenocopy the toxin. Sure enough, sustained 24h incubation with APH induced RINGs (**Fig 4E, 4F**), many of which contained RPA foci (**Fig 4E, 4G**) mirroring the toxin phenotype (**Fig 3C, Supplementary Fig 10F, 10G**). When APH was removed and cells allowed to recover, neither RPA foci nor RINGs were observed at 24h establishing that RINGs are triggered by persistent replication stress (**Fig 4E-G**). When we added toxin^{WT} to APH-treated cells, no additive effect on RPA was observed indicating the pool of RPA was already fully sequestered on ssDNA substrate (**Fig 4G**). The data supports a virulence mechanism by which the toxin overwhelms the RPA response by oversupply of ssDNA, which causes RINGs.

RING-induction by the toxin drives cells into senescence.

We next addressed the biological significance of RINGs. Induction of RPA exhaustion by replication inhibitors causes replication catastrophe and represents a 'point of no return' for cell proliferation, leading to cells acquiring senescent traits[44, 46]. Senescence is a phenotype associated with ageing that arises from stress such as persistent DNA damage and underlies multiple age-related pathologies[4]. We thus investigated whether RPA exhaustion by the toxin led to cells acquiring senescent traits[47]: permanent cell-cycle arrest, nuclear distension and augmented lysosomal content (e.g. senescence-associated beta-galactosidase; SA-β-Gal).

We first examined permanent cell-cycle arrest (**Fig 5A**). While untreated and toxin^{HQ}-treated cells proliferated, cells intoxicated with toxin^{WT} for 2h failed to re-enter the cell cycle and generate cell colonies over 7-days (top panel). Closer inspection revealed toxin^{WT}-arrested cells that were substantially enlarged relative to controls cells (arrows in bottom panel), which is consistent with previous reports citing cellular distension[12]. Toxin^{WT}-treated cells also showed augmented SA-β-Gal (**Fig 5B**), which increased from ~40% of cells on day 1 to ~80% by day 6 (**Fig 5C**).

We next examined whether the senescence-like phenotype was associated with RING formation. First, we observed toxin-induced SA-β-Gal activity in RING cells directly (blue arrows) but not in cells without DNA damage or nuclear distension (white arrows) (**Fig 5D, Supplementary Figure 11A**). Though serum-starvation is still permissive for SA-β-Gal[48], we still found that the absence of serum, a condition that blocks RING formation (**Fig 2**), significantly impaired toxin-induced SA-β-Gal activity further supporting RING-driven senescence. We hypothesised that residual SA-β-Gal in intoxicated serum-starved cells in **Fig 5E** was mediated by quiescent cells in G0 and senescent cells arrested in G1 with γH2AX foci (**Fig 2E, Supplementary Figure 6A**). Indeed, in addition to RINGs, single cell analysis also revealed SA-β-Gal activity in cells with γH2AX foci (**Supplementary Figure 11A**: white arrow) indicating that the toxin drives a senescence-like phenotype via γH2AX RINGs and foci. Senescence via RINGs was further established by increased SA-β-Gal in RING-inducing conditions via siRPA (**Fig 5F**), APH treatment (**Fig 5G**) and infection (**Fig 5H**). Taken together, these results show that RING formation is associated with a senescence-like phenotype.

The toxin induces transmissible senescence driving infection.

We next sought to establish whether the typhoid toxin transmits a senescence-associated secretory phenotype (SASP). SASP is a hallmark of cellular senescence characterised by the secretion of proteins into the extracellular milieu that induce secondary senescence and remodel the functions of bystander cells and tissues[4]. To address toxin-induced SASP (henceforth txSASP), we harvested conditioned cell culture medium from intoxicated cells or *Salmonella*-infected cells before adding the medium to fresh cells and phenotyping as depicted in **Fig 5I**. Remarkably, conditioned medium originating from toxin-treated (tox^{WT}) or wild-type infected (Sm^{WT}) cells transmitted a senescent-like phenotype to freshly seeded cells (**Fig 5J**). In contrast, conditioned medium from cells treated with the toxin null strain had no effect (**Fig 5J;** $Sm^{\Delta cdtB}$). Moreover, successive batches of conditioned medium originating from the Sm^{WT}-infected cells could also induce txSASP in ~70% of cells (**Supplementary Fig 11B-D**). This provides additional evidence of a transmissible senescence-like phenotype whilst also controlling for any toxin secreted by intracellular *Salmonella* during the initial infection (depicted in **Supplementary Fig 11B**). Consistent with txSASP, conditioned medium from tox^{WT}- but not tox^{HQ}-cells caused a significant DDR (**Fig 5K**). We also confirmed that phenotypes were not due to contaminating toxin in conditioned media as wash fractions (depicted in **Fig 5I**) were incapable of triggering a γH2AX DDR when added to fresh cells (**Supplementary Fig 11E**).

The significance of senescence to host-pathogen interactions is not understood. To investigate whether txSASP influences infection, we treated THP1 cells with conditioned

medium 6-days before infection and assaying intracellular *Salmonella* at 24h (**Fig 5L**). We found that txSASP promoted infection (tox^{WT}) relative to cells treated with control conditioned medium (untreated or tox^{HQ}). TxSASP enhanced *Salmonella* invasion into host cells (**Supplementary Fig 12A, 12B**), which was enhanced by conditioned medium obtained in RING permissive conditions (+serum) (**Supplementary Fig 12C**). Interestingly, SASP by RING-inducers APH and siRPA was markedly reduced relative to the toxin (**Supplementary Fig 12D**: APH 40%, siRPA 50%; **Fig 5J**: toxin, 80%) and no significant increase in invasion was observed (**Supplementary Fig 12E**) indicating that the mode of RPA exhaustion elicited by the toxin initiates a robust SASP, which promotes invasion. These results show that the typhoid toxin triggers a non-canonical DDR that elicits a pathogen-associated senescence-like phenotype, which further drives intracellular *Salmonella* infections by inducing transmissible senescence.

Discussion

γH2AX is a central hub in the DDR that orchestrates DNA repair and cell fate. Here, we report a non-canonical DDR response characterised by signature accumulation of γH2AX at the nuclear periphery – the RING phenotype - generated via ATR at heterochromatin. Non-canonical γH2AX localisation at the nuclear periphery has been observed in apoptosis[32, 33]. This contrasts with the RING phenotype that represents a discrete branch of γH2AX signalling marking replication stress and entry into a senescence-like state.

We uncover that pathogens overwhelm the RPA response to DNA damage. RPA knockdown induced RINGs while increasing RPA expression counteracted the toxin as RINGs were inhibited. Thus, RPA represents a safeguard against RINGs. The cell has a finite pool of RPA for stoichiometric interactions with ssDNA[44], and ssDNA could be left unprotected by (i) low levels of RPA itself (i.e. knockdown experiments), or (ii) high levels of ssDNA generated via a toxin. We show that toxin endonuclease activity elevated the amount of unprotected ssDNA, which sequestered RPA. Consistent with toxin manipulation of RPA, related CDTs induce single-strand DNA breaks *in vitro*[19, 20], as well as accumulate ssDNA and RPA foci in cells[21]. Since heterochromatin is refractory to γH2AX production until its decompaction for DNA replication late in S-phase[1, 39, 40], it is likely that insufficient RPA late in S-phase induces DNA damage manifesting as γH2AX RINGs at the nuclear periphery. Thus, our data support a model (**Fig 6**) whereby the damage *caused* by the toxin in G1 and S-phase is targeted by RPA (**Fig 6D**), which is observed as RPA foci. The damage observed in γH2AX RINGs however is different: this damage is a *consequence* of RPA exhaustion in S-phase, insufficient RPA, which is supported by our observations that (i) RPA is absent from RINGs, and (ii) RPA knockdown is sufficient to induce γH2AX RINGs (**Fig 6E**). Together, the data implicate the typhoid toxin and CDTs in pathogen-mediated RPA exhaustion, a virulence mechanism transmitting a senescence-like phenotype that enhances infection (**Fig 6F**).

Senescence is a characteristic feature of ageing associated with impaired responses to pathogens[49], yet whether pathogenic bacteria exploit senescence is unclear. We propose that the physiological role of the RING is to induce a senescent-like response to RPA exhaustion, which is hijacked by *Salmonella*. RING cells exhibited senescence-like traits including permanent cell-cycle arrest, persistent DNA damage, augmented lysosomal activity, plus cell and nuclear distension, which have been observed in senescent cells in response to diverse stimuli[47]. Moreover, the toxin triggered senescence in cells directly (i.e. infection, intoxication) and indirectly through txSASP that transmitted the senescence-like effect. Intriguingly, aged animals have been found more susceptible to infections by

Salmonella Typhimurium[50] and methicillin-resistant *Staphylococcus aureus*[51]. Consistent with this, toxin-dependent transmittable senescence increased host cell susceptibility to *Salmonella* invasion. Nevertheless, whether RINGs occurs *in vivo* remains to be established: *Salmonella* is known to colonise intestinal crypts, bone marrow, liver and spleen[17, 52] that are rich in proliferating cells (i.e. RING-permissive), which could be targeted by secreted toxin. Indeed, secreted typhoid toxin has been localised in the liver where the toxin caused chronic *Salmonella* carriage in an animal infection model[14]. Thus, genotoxic *Salmonella* (e.g. *S.*Typhi, *S.*Paratyphi, *S.*Javiana) could deploy the toxin to subvert senescence in local cellular populations to cause disease, e.g. in chronic human infections[52]. This could be extended to diverse pathogens encoding CDTs that can promote senescence-like phenotypes[53, 54].

We reveal a non-canonical DDR, the RING phenotype, triggered by bacterial manipulation of the ssDNA-sensor RPA that causes a senescence-like phenotype to drive *Salmonella* infections. The work uncovers a function of the typhoid toxin that could be of significance to globally important infectious diseases.

Methods

Plasmids and recombinant toxin purification

The plasmid peGFP-C1 encoding *pltB*^{His} *pltA*^{Myc} and *cdtB*^{FLAG} (kind gift from Prof.Teresa Frisan, Umeå) was used to amplify epitope-tagged *pltBA* (PltB_Nco1_FWD 5'-GAGCCCCATGGGCTATATGAGTAAGTATGTACCTG-3'/PltA_Myc_EcoR1_REV 3'-CGGCCGAATTCTTACAGGTCTTCTTCAGAGATCAG-5') and *cdtB* (CdtB_Nde1_FWD 5'-GATATACATATGAAAAAACCTGTTTTTTTCCTTC-3'/CdtB_FLAG_Xho1_REV 3'-GGCCACTCGAGTTACTTGTCATCGTCGTCCTTGTA-5') by polymerase chain reaction (PCR) using Phusion Polymerase (NEB). pETDuet-1 encoding toxin^{WT} was generated by digesting PCR product *pltBA* and plasmid pETDUet-1-MCS1 using Nco1/EcoR1 restriction endonucleases and *cdtB*/pETDUet-1-MCS2 using Nde1/Xho1 before ligation with T4 DNA ligase according to manufacturer instructions (NEB). The point mutation H160Q was introduced into *cdtB* by PCR site-directed mutagenesis to generate toxin^{HQ} (CdtB_H160Q_F 5'-GTTTTTCTGACAGCGCAGGCACTGGCTAGTGGAG-3'/CdtB_H160Q_R 3'-CTCCACTAGCCAGTGCCTGCGCTGTCAGAAAAAC-5'). The plasmid pGEM CDT-I ABC encoding the EcCDT-1 of *E. coli* (strain E6468/62 O86: H34) was a kind gift from Prof. Eric Oswald, Toulouse and was used to amplify epitope-tagged *cdtAB* (ecCdtA_Nco1_F 5'-GGGCCCCATGGATAAAAAACTAATTGCATTTTTGTGC-3'/ecCdtB_Myc_EcoR1_R 3'-CGGCCGAATTCTCACAGATCCTCTTCTGAGATGAGTTTTTGTTCTCTTCTTGCTCCTCTTCCAG GAATAAAGC-5') and *cdtC* (ecCdtC_Nde1_F 5-GATATACATATGAAAACAGTTATAGTACTTTTTGTTTTACTGC-3'/ecCdtC_His_Xho1_R 3'-GGCCACTCGAGTCAGTGGTGGTGGTGGTGGTGGCTCGTTAATGGAGACATTATTGCCGG-5') before cloning of EcCDT-1 into pETDuet-1 as typhoid toxin. Recombinant His-tagged toxins were expressed overnight in *E.coli* BL21 DE3 (#69450, Merck Millipore) at 30˚C following addition of 0.1mM Isopropyl β-D-1-thiogalactopyranoside (Sigma-Aldrich). *E.coli* were harvested by centrifugation and resuspended in lysis buffer containing 20mM Tris-HCl, pH 8.0, 100mM NaCl, 1mM $MgCl_2$ (Sigma-Aldrich) and complete EDTA-free protease inhibitor cocktail (Roche) then lysed by passage through a Cell Disrupter at 30kPSI (Constant systems Ltd). His-tagged toxin was purified from the lysate using NiNTA agarose (Qiagen) via affinity chromatography according to manufacturer instructions and stored at -80˚C in lysis buffer supplemented with 20% glycerol.

Antibodies and immunoblotting

Antibodies were purchased from Abcam (Salmonella diluted 1:1000, ab35156; RPA70/1:1000, ab79398; RPA32/RPA2/1:1000, ab16850; RPA32pT21/pRPA/1:1000, ab61065; tubulin/1:1000, ab7291/ab52866; H3K9me3/1:1000, ab176916), Cell Signalling Technology (diluted 1:500 CHK1-pS345, 2341; CHK2-pT68/1:500, 2197; ATR-pS428/1:500, 2853; ATM pS1981/1:500, 5883;cleaved PARP1/1:500, 5625; cleaved caspase-3/1:250, 9664; γH2AX/1:1000, 9718), Bethyl laboratories (RPA32 diluted 1:1000, A300-244A; RPA32-pS33/pRPA32/1:1000, A300-246A), Sigma (FLAG M2 diluted 1:1000, F3165), GenScript (Myc diluted 1:1000, A00172-200), Qiagen

(His diluted 1:1000, 34660), Millipore (yH2AX diluted 1:1000, 05-636-I), Novusbio (53BP1 diluted 1:1000, NB100-304), BD Bioscience (BrdU diluted 1:200, 347580). Secondary antibodies were diluted 1:10000 and purchased from ThermoFisher Scientific (Alexa 488 donkey anti-mouse IgG, A-21202; Alexa 594 donkey anti-rabbit IgG, A-21207) for immunofluorescence microscopy and LiCor Biosciences (IRDye® 800CW Donkey anti-Mouse IgG, 925-32212; IRDye® 680RD Donkey anti-Rabbit IgG, 926-68073) for immunoblotting. Proteins were separated by 9% Bis-Tris SDS-PAGE gels in MOPS buffer (50 mM MOPS, 50 mM Tris, 0.1% SDS, 20 mM EDTA) and transferred to PVDF transfer stacks using iBlot 2 (Thermo Fisher Scientific). Immunoblotting was performed with Odyssey Blocking buffer (PBS) and IRDye-labelled secondary antibodies according to manufacturer's instructions (LiCor). The unprocessed source data for immunoblots are in the Source Data file.

Intoxication assay and drug treatments

Approximately $5x10^4$ mammalian cells were seeded onto glass coverslips (30% confluency) the day before intoxication with 5ng/ml recombinant typhoid toxin for 2h at 37˚C. Cells were washed and further incubated, typically 24h, in complete growth media before phenotypic analysis. Drugs were incubated with cells as indicated in the text or 1h before intoxication when used in combination with the typhoid toxin and remained present throughout experiments. 20μM Aphidicolin (A0781, Sigma-Aldrich), 1μM Killer-TRAIL (ALX-201-073-CO20, Enzo), 100nM staurosporine (SM97-1 Cambridge Bioscience), 30μM Z-VAD-OMe-FMK (Selleckchem), 10μM iATM KU55933, 15μM iATR NU6072 (Tocris).

Cell culture and siRNA transfection

HT1080 (#ATCC® CCL-121), RAW 264.7 (#ATCC® TIB-71™), CACO2 (#ATCC® HTB-37), HAP1 (Horizon Discovery Group) and MEF (#ATCC® SCRC-1008™) cells were cultured (37˚C, 5% CO_2) in DMEM (Sigma), HIEC-6 (#ATCC® CRL-3266) cells in OptiMEM 1 Reduced Serum Medium (Gibco), THP1s (#ATCC® TIB-202™) in RPMI1640, and U-2-OS (ATCC identifier HTB-96) cells in McCoy's 5A Medium (Gibco). Growth media was supplemented with 200μg/ml^{-1} streptomycin and 100Uml^{-1} penicillin (Sigma), 2mM L-Glutamine, and 10% heat-inactivated foetal calf serum (FCS) (Lonza). U-2-OS control cells and U-2-OS cells stably expressing ~2-fold excess of all three RPA subunits via acGFP-RPA3-P2A-RPA1-P2A-RPA2[44] were a kind gift from Prof. Luis Toledo, Copenhagen. THP1 monocytes were differentiated into macrophage-like cells by stimulation with 100ng/ml Phorbol 12-myristate 13-acetate (PMA) for 3 days then cultured for an additional day without PMA before experiments. Cells were arrested in G_1 phase by serum-starvation in serum-free culture medium 24h before and during experiments. The following were used used according to manufacturer instructions: Click-iT EdU Alexa Fluor 647 Imaging Kit and BrdU (Thermo Fisher Scientific), and the Cellular Senescence Detection Kit - SPiDER-ßGal (DOJINDO). ON-Target Plus RPA1 (L-015749-01-0005), ATR (L-003202-00-0005), ATM (L-003201-00-0005) and GAPDH (D-

001830-01-05) siRNAs were transfected into cells using DharmaFECT1 (0.25µl per well of 24-well plate) according to the manufacturer's instructions (Dharmacon) 48h before experiments.

Salmonella strains and infection

*S.*Javiana (S5-0395) and Δ*cdtB* (M8-0540)[15, 16] were kind gifts from Prof. Martin Weidmann (New York). *S.*Typhi Ty2 vaccine strain BRD948[55] (kind gift from Prof. Gordon Dougan, Cambridge). The lambda Red recombinase system[56] was used to create *S.*Typhi Δ*cdtB*: primers cdtB_FRT_F 5'-ATGAAAAAACCTGTTTTTTTCCTTCTGACCATGATCATCTTGTGTAGGCTGGAGCTGCTTC-3'/cdtB_FRT_R 3'-TTAACAGCTTCGTGCCAAAAAGGCTACGGGATAATGATCACATATGAATATCCTCCTTAG-5' were used to amplify a kanamycin-resistance cassette from plasmid pKD4 flanked by FLP (recombinase) recognition target (FRT) sites and ~40 nucleotide extensions homologous to *cdtB*. The construct was transformed into *S.*Typhi expressing λ red recombinase from the plasmid pKD46 and Δ*cdtB* transformants cultured overnight at 37˚C on LB agar plates supplemented with 50µg/ml kanamycin. Gene knockout of *cdtB* was confirmed by colony PCR using primers flanking *cdtB* 68_cdtB_upstream_F 5'-GCACCTTACGCTCAAAG-3'/60_sty1887_3'_R 5'-GAGTTGTTTTACCAGTC-3'. Kanamycin-resistant Δ*cdtB* transformants were streaked out onto LB plates without antibiotics and incubated overnight at 42˚C to cure pKD46. For infections, $1x10^5$ of indicated cultured cells were infected with *Salmonella* strains (MOI of 5) for 30min, washed, and then incubated in growth media supplemented with 10µg/ml gentamicin to kill extracellular bacteria. When appropriate, conditioned media from *Salmonella*-infected cells was harvested at 48h and filter-sterilised before incubation with naïve cultured cells. In microscopy experiments, *Salmonella* were labelled with anti-*Salmonella* antibodies. *Salmonella* invasion was assayed by lysing cells in 0.5% TritonX-100 before culturing *Salmonella* by spotting 10µl of serially-diluted whole cell lysates on LB agar plates and incubating overnight at 37˚C. The number of *Salmonella* colony forming units (CFUs) were calculated from bacterial colony counts.

Immunofluorescence microscopy

Cultured cells on coverslips were fixed by incubation in PBS containing 4% PFA. For immunofluorescence, cells were blocked in PBS 3% BSA 0.2% TritonX-100 and incubations with antibodies performed in PBS 0.2% TritonX-100. DNA was stained with DAPI 6µg/ml for 3 min. For RPA staining, cultured cells were extracted in PBS 0.1% Tween for 1 min on ice before fixation. Non-differentiated THP1s were fixed and stained in suspension and centrifuged onto microscopy slides for 6 min at 4000 rpm with a cytospin (Shandon Southern Instruments). Coverslips were mounted on slides using VectaShield Antifade Mounting Medium (Vector Laboratories) and sealed with nail varnish. Images were taken on a Nikon Eclipse Ti microscope and collected with a SCMOS camera (Andor Zyla) using NIS-Elements Advanced Research software (Nikon). Quantitative analysis followed high-content immunofluorescence microscopy of cells in 96-well

Flat-bottomed μCLEAR plates (Greiner CELLSTAR) with images taken on a Molecular Devices ImageXpress Microscope using MetaXpress 3.1 software. For high resolution immunofluorescence microscopy, cells were seeded on high precision 22 mm x 22 mm cover glasses (Paul Marienfeld GmbH & Co. KG), before imaging on an OMX Deltavision structured illumination microscope or a Zeiss AiryScan confocal microscope (LSM 880) using the Zeiss Zen Software. Microscopy images were processed in ImageJ and figures assembled in Adobe Illustrator. The unprocessed source data for images are in the Source Data file.

RING Tracking

For automated analysis of DNA damage phenotypes, a custom-made script was developed in MATLAB (http://uk.mathworks.com/products/matlab/) to analyse 20x objective images. First, nuclei were detected using the DAPI channel image: the original image was filtered with a 2-D Gaussian smoothing kernel, which was used to create a binary image with a globally automatically determined threshold. A series of dilation, hole filling and eroding was applied to the binary image with parameters initially manually adjusted by the investigator and then fixed throughout the analysis. The resulting image was used to detect objects, which were filtered by their area (greater than 400px), eccentricity (less than 0.8), shape regularity (4**Area^2/Perimeter >0.85), and signal intensity (less than 2*Median Intensity of all objects) to exclude all objects that did not represent nuclei. To classify nuclei by γH2AX distribution, the γH2AX signal in each nucleus was binarised with an adaptive threshold, which uses local first-order image statistics around each pixel. This allowed an efficient detection of foci even in the presence of high background. The nuclei with number of foci divided by the nucleus area being greater than 0.0035 were considered as having foci γH2AX distribution. The nuclei with non-foci γH2AX distribution were then further classified into uniform and RING phenotypes. Namely, the profiles of γH2AX intensity from the centre of mass of each object to each pixel at the object boundary were created. These profiles were then resampled to be of the same length, equal to their maximum length, and averaged to create an average radial intensity profile for each nucleus. The nucleus was classified as a RING if the difference between mean intensity in its last quartile and first three quartiles was greater than 10% of overall mean intensity. All above cut-off values were determined empirically by testing images from different experiments and identifying a combination, which was the most efficient in detecting and classifying nuclei. Finally, the correlation between γH2AX and 53BP1 signal was determined by calculating the pairwise correlation coefficient between their intensities at each pixel within individual nuclei.

Flow cytometry

Cells were collected with a cell scraper, washed in PBS, and fixed in ice-cold 70% ethanol in PBS on ice for 30 min. Cells were incubated in flow cytometry buffer (PBS, 100 µg/ml RNase, 40 µg/ml propidium iodide, Sigma) for 30 min at 37˚C in the dark to degrade RNA. At least 15,000 cells per sample were subsequently analysed on a FACSCalibur Flow Cytometer (Beckman Coulter). Experiments were done in duplicates and repeated at least 3 times. Analysis was performed with FlowJo Software.

Clonogenic survival assay

Cells were seeded at $2x10^3$ cells per 10 cm dish 24h before intoxication assays. After 8 days, cells were washed with PBS, fixed for 15 min in 80% ethanol, air-dried and stained with 1% methylene blue for 1h. Plates were rinsed, dried, and colonies were counted.

Senescence assays

To visualise senescent-like cells, a Senescence-Galactosidase Staining Kit (Cell Signaling Technology, 9860) was used according to manufacturer's instruction. The staining was carried out at pH 6.0 in a humidified chamber overnight at 37˚C. Imaging was carried out using an Olympus wide field microscope CK30 10x objective and captured with Dino-Lite adaptor and Dino-Lite software. For SASP experiments, conditioned medium cells was harvested from intoxicated HT1080 cells at 4 days, unless indicated otherwise, and filter sterilised before incubation with naïve HT1080 cells or non-differentiated THP1s. Cells were incubated for 7 days before assaying DNA damage, infection or SA-β-Galactosidase activity.

Nuclease assays

Reactions were prepared on ice and contained Digestion buffer (final concentration 25mM HEPES pH 7.0, 4mM $MgCl_2$, 4 mM $CaCl_2$) supplemented with 300ng pET-Duet1 plasmid DNA and indicated amounts of nuclease. 1U of bovine DNase (Sigma) was used as a positive control. Reactions were performed at 37˚C and stopped by addition of 10x Quench buffer (final concentration 16mM EDTA, 6% glycerol) before heat inactivation at 75˚C. 100ng of plasmid DNA was analysed on 0.8% agarose gels buffered in TBE pH8.0 (89mM Tris, 89mM Boric acid, 2mM EDTA). The unprocessed source data for agarose gels are in the Source Data File.

RPA-protection assay

Toxin- or aphidicolin-treated cells immobilised on glass coverslips were washed in PBS, permeabilised in PBS 0.1 % Tween for 1 min on ice, then fixed in PBS 4% PFA at room tempertaure. Cells were inverted onto 50µl DNA polymerase reaction mix containing One-Taq Hot Start polymerase (Bioline, M0481G), 0.4 mM BrdU, 0.2mM dNTP (Bioline) and incubated for 5 min at 72˚C in a water-bath. Cells were returned to ice and washed with PBS before 20min

permeabilisation with PBS 0.2% TritonX-100. BrdU-labelled DNA double strands were denatured for 30 min with 1N HCl, washed with PBS, then BrdU labelled by anti-BrdU antibodies before immunofluorescence microscopy.

Alkaline Comet assay

Cells seeded in 6-well plate (100,000 per well) were treated with typhoid toxin and incubated at 37°C to permit DNA damage. Cells were harvested using a cell scraper in ice-cold PBS. Cells were combined 1:1 with 1.2% agarose (150µl) and loaded onto 0.6% agarose (150µl) immobilised on fully-frosted glass slides then topped with coverglass. Cells were lysed in lysis buffer (10mM Tris pH10, 100mM EDTA, 2.5M NaCl, 1% Tx100. 1% DMSO) for 1h, 4°C. Agarose gel electrophoresis was performed for 25min at 12V in electrophoresis buffer (10mM Tris pH10, 1mM EDTA, 10mM NaOH, 1% DMSO). DNA was labelled with SYBR green solution (Invitrogen, S7563). Comets were scored on a microscope with a 10x Plan Fluor objective on Nikon inverted microscope and analysed with software Comet Assay IV (Instem).

Data analysis and statistics

Data analysis was performed in Microsoft Excel. Statistical analysis was performed using Prism 7 Graphpad software. Biological replicates are independent experiments. Technical replicates or fields of view indicate analysis of the same experiment. Non-significant is marked as ns in figures and legends.

Data availability

The authors declare that data supporting the findings of this study are available within the paper and its supplementary information files. A reporting summary for this manuscript is available as a Supplementary Information file. The source data underlying mean values, gel, blot and fluorescence images in main Figures 1-5, and Supplementary Figures 1-12 are provided as a Source Data file. All new data associated with the manuscript will be made publicly available on Figshare (https://figshare.shef.ac.uk/s/60e5c9808685265f687c) and can be identified using the title of the manuscript as a search term.

Code availability statement

The code for RING Tracking is publicly available on: https://github.com/nbul/Nuclei.

Reporting Summary

Further information on research design is available in the Nature Research Reporting Summary linked to this article.

References

1. Polo SE, Jackson SP. Dynamics of DNA damage response proteins at DNA breaks: a focus on protein modifications. *Genes Dev* **25**, 409-433 (2011).

2. Celeste A*, et al.* Histone H2AX phosphorylation is dispensable for the initial recognition of DNA breaks. *Nat Cell Biol* **5**, 675-679 (2003).

3. Yuan J, Adamski R, Chen J. Focus on histone variant H2AX: to be or not to be. *FEBS Lett* **584**, 3717-3724 (2010).

4. Hernandez-Segura A, Nehme J, Demaria M. Hallmarks of Cellular Senescence. *Trends Cell Biol* **28**, 436-453 (2018).

5. Cimprich KA, Cortez D. ATR: an essential regulator of genome integrity. *Nat Rev Mol Cell Biol* **9**, 616-627 (2008).

6. Wold MS. Replication protein A: a heterotrimeric, single-stranded DNA-binding protein required for eukaryotic DNA metabolism. *Annu Rev Biochem* **66**, 61-92 (1997).

7. Zou L, Elledge SJ. Sensing DNA damage through ATRIP recognition of RPA-ssDNA complexes. *Science* **300**, 1542-1548 (2003).

8. Fanning E, Klimovich V, Nager AR. A dynamic model for replication protein A (RPA) function in DNA processing pathways. *Nucleic Acids Res* **34**, 4126-4137 (2006).

9. Burma S, Chen BP, Murphy M, Kurimasa A, Chen DJ. ATM phosphorylates histone H2AX in response to DNA double-strand breaks. J Biol Chem. Preprint at https://www.ncbi.nlm.nih.gov/pubmed/11571274 (2001).

10. Ward IM, Chen J. Histone H2AX is phosphorylated in an ATR-dependent manner in response to replicational stress. J Biol Chem. Preprint at https://www.ncbi.nlm.nih.gov/pubmed/11673449 (2001).

11. Weitzman MD, Weitzman JB. What's the damage? The impact of pathogens on pathways that maintain host genome integrity. *Cell Host Microbe* **15**, 283-294 (2014).

12. Spano S, Ugalde JE, Galan JE. Delivery of a Salmonella Typhi exotoxin from a host intracellular compartment. *Cell Host Microbe* **3**, 30-38 (2008).

13. Song J, Gao X, Galan JE. Structure and function of the Salmonella Typhi chimaeric A(2)B(5) typhoid toxin. *Nature* **499**, 350-354 (2013).

14. Del Bel Belluz L*, et al.* The Typhoid Toxin Promotes Host Survival and the Establishment of a Persistent Asymptomatic Infection. *PLoS Pathog* **12**, e1005528 (2016).

15. Miller RA, Wiedmann M. The Cytolethal Distending Toxin Produced by Nontyphoidal Salmonella Serotypes Javiana, Montevideo, Oranienburg, and Mississippi Induces DNA Damage in a Manner Similar to That of Serotype Typhi. MBio. Preprint at https://www.ncbi.nlm.nih.gov/pubmed/27999166 (2016).

16. Miller RA, Betteken MI, Guo X, Altier C, Duhamel GE, Wiedmann M. The Typhoid Toxin Produced by the Nontyphoidal Salmonella enterica Serotype Javiana Is Required for Induction of a DNA Damage Response In Vitro and Systemic Spread In Vivo. MBio. Preprint at https://www.ncbi.nlm.nih.gov/pubmed/29588404 (2018).

17. Dougan G, Baker S. Salmonella enterica serovar Typhi and the pathogenesis of typhoid fever. *Annu Rev Microbiol* **68**, 317-336 (2014).

18. Guidi R, Levi L, Rouf SF, Puiac S, Rhen M, Frisan T. Salmonella enterica delivers its genotoxin through outer membrane vesicles secreted from infected cells. *Cell Microbiol* **15**, 2034-2050 (2013).

19. Elwell CA, Dreyfus LA. DNase I homologous residues in CdtB are critical for cytolethal distending toxin-mediated cell cycle arrest. *Mol Microbiol* **37**, 952-963 (2000).

20. Nesic D, Hsu Y, Stebbins CE. Assembly and function of a bacterial genotoxin. *Nature* **429**, 429-433 (2004).

21. Fedor Y*, et al.* From single-strand breaks to double-strand breaks during S-phase: a new mode of action of the Escherichia coli Cytolethal Distending Toxin. *Cell Microbiol* **15**, 1-15 (2013).

22. Frisan T, Cortes-Bratti X, Chaves-Olarte E, Stenerlow B, Thelestam M. The Haemophilus ducreyi cytolethal distending toxin induces DNA double-strand breaks and promotes ATM-dependent activation of RhoA. *Cell Microbiol* **5**, 695-707 (2003).

23. Nougayrede JP*, et al.* Escherichia coli induces DNA double-strand breaks in eukaryotic cells. *Science* **313**, 848-851 (2006).

24. Fahrer J*, et al.* Cytolethal distending toxin (CDT) is a radiomimetic agent and induces persistent levels of DNA double-strand breaks in human fibroblasts. *DNA Repair (Amst)* **18**, 31-43 (2014).

25. Frisan T. Bacterial genotoxins: The long journey to the nucleus of mammalian cells. Biochim Biophys Acta. Preprint at https://www.ncbi.nlm.nih.gov/pubmed/26299818 (2016).

26. Humphreys D, Davidson A, Hume PJ, Koronakis V. Salmonella virulence effector SopE and Host GEF ARNO cooperate to recruit and activate WAVE to trigger bacterial invasion. *Cell Host Microbe* **11**, 129-139 (2012).

27. Humphreys D, Davidson AC, Hume PJ, Makin LE, Koronakis V. Arf6 coordinates actin assembly through the WAVE complex, a mechanism usurped by Salmonella to invade host cells. *Proc Natl Acad Sci U S A* **110**, 16880-16885 (2013).

28. Haghjoo E, Galan JE. Salmonella typhi encodes a functional cytolethal distending toxin that is delivered into host cells by a bacterial-internalization pathway. *Proc Natl Acad Sci U S A* **101**, 4614-4619 (2004).

29. den Bakker HC*, et al.* Genome sequencing reveals diversification of virulence factor content and possible host adaptation in distinct subpopulations of Salmonella enterica. BMC Genomics. Preprint at https://www.ncbi.nlm.nih.gov/pubmed/21859443 (2011).

30. Li L*, et al.* The Haemophilus ducreyi cytolethal distending toxin activates sensors of DNA damage and repair complexes in proliferating and non-proliferating cells. *Cell Microbiol* **4**, 87-99 (2002).

31. Pons BJ*, et al.* Cell transfection of purified cytolethal distending toxin B subunits allows comparing their nuclease activity while plasmid degradation assay does not. Plos One. Preprint at <Go to ISI>://WOS:000462594000053 (2019).

32. Solier S, Sordet O, Kohn KW, Pommier Y. Death receptor-induced activation of the Chk2- and histone H2AX-associated DNA damage response pathways. *Mol Cell Biol* **29**, 68-82 (2009).

33. Solier S*, et al.* Heat shock protein 90alpha (HSP90alpha), a substrate and chaperone of DNA-PK necessary for the apoptotic response. *Proc Natl Acad Sci U S A* **109**, 12866-12872 (2012).

34. Sewerynek E, Ortiz GG, Reiter RJ, Pablos MI, Melchiorri D, Daniels WMU. Lipopolysaccharide-induced DNA damage is greatly reduced in rats treated with the pineal hormone melatonin. *Mol Cell Endocrinol* **117**, 183-188 (1996).

35. Mack L, Brill B, Delis N, Groner B. Endotoxin depletion of recombinant protein preparations through their preferential binding to histidine tags. *Anal Biochem* **466**, 83-88 (2014).

36. Cheng R, Choudhury D, Liu C, Billet S, Hu T, Bhowmick NA. Gingival fibroblasts resist apoptosis in response to oxidative stress in a model of periodontal diseases. Cell Death Discov. Preprint at <Go to ISI>://WOS:000463069500041 (2015).

37. Miller R, Wiedmann M. Dynamic Duo-The Salmonella Cytolethal Distending Toxin Combines ADP-Ribosyltransferase and Nuclease Activities in a Novel Form of the Cytolethal Distending Toxin. Toxins (Basel). Preprint at https://www.ncbi.nlm.nih.gov/pubmed/27120620 (2016).

38. Pellegrino S, Michelena J, Teloni F, Imhof R, Altmeyer M. Replication-Coupled Dilution of H4K20me2 Guides 53BP1 to Pre-replicative Chromatin. *Cell Rep* **19**, 1819-1831 (2017).

39. Gilbert DM. Replication timing and transcriptional control: beyond cause and effect. *Curr Opin Cell Biol* **14**, 377-383 (2002).

40. Kim JA, Kruhlak M, Dotiwala F, Nussenzweig A, Haber JE. Heterochromatin is refractory to gamma-H2AX modification in yeast and mammals. *Journal of Cell Biology* **178**, 209-218 (2007).

41. Olson E, Nievera CJ, Klimovich V, Fanning E, Wu X. RPA2 is a direct downstream target for ATR to regulate the S-phase checkpoint. *J Biol Chem* **281**, 39517-39533 (2006).

42. Oakley GG, Patrick SM. Replication protein A: directing traffic at the intersection of replication and repair. *Front Biosci (Landmark Ed)* **15**, 883-900 (2010).

43. Murphy AK*, et al.* Phosphorylated RPA recruits PALB2 to stalled DNA replication forks to facilitate fork recovery. *J Cell Biol* **206**, 493-507 (2014).

44. Toledo LI*, et al.* ATR prohibits replication catastrophe by preventing global exhaustion of RPA. *Cell* **155**, 1088-1103 (2013).

45. Zellweger R*, et al.* Rad51-mediated replication fork reversal is a global response to genotoxic treatments in human cells. *Journal of Cell Biology* **208**, 563-579 (2015).

46. Toledo L, Neelsen KJ, Lukas J. Replication Catastrophe: When a Checkpoint Fails because of Exhaustion. *Mol Cell* **66**, 735-749 (2017).

47. Sharpless NE, Sherr CJ. Forging a signature of in vivo senescence. *Nat Rev Cancer* **15**, 397-408 (2015).

48. Yang NC, Hu ML. The limitations and validities of senescence associated-beta-galactosidase activity as an aging marker for human foreskin fibroblast Hs68 cells. *Exp Gerontol* **40**, 813-819 (2005).

49. Shaw AC, Goldstein DR, Montgomery RR. Age-dependent dysregulation of innate immunity. *Nat Rev Immunol* **13**, 875-887 (2013).

50. Bradley SF, Kauffman CA. Aging and the response to Salmonella infection. *Exp Gerontol* **25**, 75-80 (1990).

51. Tseng CW, Kyme PA, Arruda A, Ramanujan VK, Tawackoli W, Liu GY. Innate immune dysfunctions in aged mice facilitate the systemic dissemination of methicillin-resistant S. aureus. PLoS One. Preprint at https://www.ncbi.nlm.nih.gov/pubmed/22844481 (2012).

52. Gunn JS, Marshall JM, Baker S, Dongol S, Charles RC, Ryan ET. Salmonella chronic carriage: epidemiology, diagnosis, and gallbladder persistence. Trends Microbiol. Preprint at https://www.ncbi.nlm.nih.gov/pubmed/25065707 (2014).

53. Blazkova H, Krejcikova K, Moudry P, Frisan T, Hodny Z, Bartek J. Bacterial intoxication evokes cellular senescence with persistent DNA damage and cytokine signalling. *J Cell Mol Med* **14**, 357-367 (2010).

54. Guidi R*, et al.* Chronic exposure to the cytolethal distending toxins of Gram-negative bacteria promotes genomic instability and altered DNA damage response. *Cell Microbiol* **15**, 98-113 (2013).

55. Lowe DC*, et al.* Characterization of candidate live oral Salmonella typhi vaccine strains harboring defined mutations in aroA, aroC, and htrA. *Infect Immun* **67**, 700-707 (1999).

56. Datsenko KA, Wanner BL. One-step inactivation of chromosomal genes in Escherichia coli K-12 using PCR products. *Proc Natl Acad Sci U S A* **97**, 6640-6645 (2000).

57. Yang YA, Chong A, Song J. Why Is Eradicating Typhoid Fever So Challenging: Implications for Vaccine and Therapeutic Design. Vaccines-Basel. Preprint at <Go to ISI>://WOS:000443934000011 (2018).

Acknowledgments

We are very grateful to Dr. Catarina Henriques (University of Sheffield) for careful reading of the manuscript and the Department of Biomedical Science (University of Sheffield) for providing a productive and supportive environment for the project. We would like to thank Prof. Gordon Dougan, Prof. Teresa Frisan, Prof. Luis Toledo and Prof. Martin Wiedmann for reagents. Microscopy was performed in the Wolfson Light Microscopy Facility using a Nikon wide-field microscope, an OMX SIM microscope (funded by Medical Research Council

SHIMA award MR/K015753/1), and an AiryScan microscope (funded by the Royal Society and the University of Sheffield). The work was funded by a Medical Research Council New Investigator Research Grant to DH (MR/M011771/2) and a British Infection Association Fellowship to AEMI (BIA-2018/FEL/AI). S.E-K is supported by a Wellcome Trust Investigator Award (215485/Z/19/Z) and a Lister Institute of Preventative Medicine Fellowship.

Author Contributions

DH supervised the study. AEMI and DH devised the concept. AEMI, DH, KN, MEG performed experiments and analysed the data. AEMI, DH, KN, SEK designed experiments. SEK designed heterochromatin and DNA comet assay experiments. NAB designed RING Tracking MATLAB algorithm . AEMI, SEK, MEG, KN helped draft and critique the manuscript for intellectual content. DH wrote the manuscript.

Declaration of Interests

The authors declare no competing interests.

FIGURE LEGENDs

Figure 1. Non-canonical DNA damage response induced by a bacterial genotoxin.

(**A**) Recombinant typhoid toxin comprising epitope-tagged $CdtB^{FLAG}$, $PltA^{Myc}$ and $PltB^{His}$ (asterisk marks *E.coli* contaminant). MW in kDa left. (**B**) Toxin immunoblotted with anti-FLAG ($CdtB^{FLAG}$, green), -Myc ($PltA^{Myc}$, red), or -His antibodies ($PltB^{His}$, green). MW in kDa left. HT1080s treated with 5ng/ml wild-type toxin ($toxin^{WT}$) or catalytically inactive $toxin^{HQ}$ for 2h before analysis at 24h as follows: (**C**) Representative cell-cycle arrest induced by $toxin^{WT}$. Propidium iodide (PI) used as DNA marker and fluorochrome (a.u, arbitrary units). Cell-cycle phases indicated. (**D**) Representative image of γH2AX (magenta) and 53BP1 (yellow) with outlines of DAPI-stained nuclei. Scale bars 50μm. (**E**) Representative confocal microscopy of γH2AX RING (magenta) and DAPI-stained nuclei (cyan). Side-panels show z-sections. Scale bars 5μm. (**F**) Proportion of cells with γH2AX RINGs and foci. Coloured circles indicate means from technical replicates (2 biological replicates, ~2000 nuclei/variable). Error bars Standard Deviation (SD). (**G**) $Toxin^{WT}$-induced γH2AX RINGs . Incubation times and concentrations indicated. 6 technical replicates, ~360 nuclei/variable (1 biological replicate). Error bars Standard Error of the Mean (SEM). (**H**) Proportion of cells with 53BP1 foci. Coloured circles indicate means from fields of view (3 biological replicates, ~2200 nuclei/variable). Error bars SEM. (**I**) Proportion of 53BP1-positive cells with γH2AX RINGs and foci. Coloured circles indicate means from technical replicates (2 biological replicates, 450 nuclei/variable). Error bars SEM. (**J**) Representative image of γH2AX RINGs (magenta) in infected cells. *Salmonella* Typhi (green) encoding the toxin (WT) or toxin null mutant (Δ*cdtB*) at 24h shown with outlines of DAPI-stained nuclei. Scale bars 50μm. (**K**) Representative image of γH2AX RINGs (magenta) in EcCDT-treated cells shown with outlines of DAPI-stained nuclei. Scale bars 25μm. In representative images (**D, J, K**) arrows indicate DNA damage RINGs (blue) and foci (white). Statistical significance (**** = P<0.0001, *** = P<0.0002, ** = P<0.0021, * = P< 0.0332, ns denotes non-significant = P>=0.05) calculated using an unpaired two-sided *t* test (**G, I**), or relative to corresponding control using one-way ANOVA and Tukey's multiple comparison test (**F, H**). Source data provided as a Source Data file.

Figure 2. RINGs are triggered during S-phase of the cell cycle.

(**A**) Proportion of toxin-induced γH2AX RINGs in non replicating (- serum, blue circle) or replicating (+serum, red circle) HT1080 cells. Untreated control cells are shown. Serum-starved cells were incubated with serum from 24h as indicated (released, green circle). Coloured circles indicate means from at least 2 biological replicates (2000 nuclei per variable). (**B**) Representative image of γH2AX RINGs -/+ serum at 24h. γH2AX labelled in magenta. Outlines of DAPI-stained nuclei shown. Scale bars 50μm. (**C**) Representative image of γH2AX RINGs in released cells. Labelled as B. Scale bars 50μm. (**D**) Representative immunoblot of toxin-induced phosphorylation of CHK1

(pCHK1) and H2AX (γH2AX) -/+ serum at 6h or 24h, or 48h (released). MW in kDa left. (**E**) Representative image of EdU-labelled DNA in γH2AX RING or foci cells at 24h. EdU incubated for 24h. Scale bars 5μm. (**F**) Proportion of γH2AX RING cells with EdU-labelled DNA at 24h. EdU incubated for 24h or 1h before fixation. Circles indicate means from at least 3 biological replicates (>220 nuclei per condition).(**G**) Representative image of γH2AX RINGs (blue arrow) or foci (white arrow) in the presence of DMSO (control), ATR inhibitor (iATR), or ATM inhibitor (iATM) shown with outlines of DAPI-stained nuclei. Toxin^{HQ} used as negative control. Scale bars 50μm. (**H**) Proportion of γH2AX RINGs in presence of ATR/ATM inhibitors at 24h. Control toxin^{HQ}-treated cells are shown. Circles indicate means from 2 biological replicates (470 nuclei per variable).
Statistical significance (**** = P<0.0001, *** = P<0.0002, ** = P<0.0021, * = P< 0.0332, ns = P>=0.05) was calculated relative to corresponding control (unt, +serum in **A**; toxin^{HQ} in **H**) using one-way ANOVA and a Tukey's multiple comparison test (**A, H**), or between samples using an unpaired two-sided *t* test (**F**). Error bars SD. Source data are provided as a Source Data file.

Figure 3. RINGs mark RPA exhaustion induced by the typhoid toxin.

(**A**) Representative immunoblot of HT1080 cells intoxicated with toxin^{WT} or toxin^{HQ} (tx^{HQ}) for 2h before analysis with indicated antibodies at time-points marked in hours (hr). MW in kDa left. (**B**) Proportion of intoxicated cells with γH2AX RINGs or γH2AX foci containing RPA pT21 foci (pRPA, grayscale). γH2AX labelled in magenta. 2 biological replicates (1500 nuclei per variable). Error bars SD. (**C**) Representative image of RPA32 pT21 (pRPA) with γH2AX RINGs (blue arrow) or foci (white arrow). Scale bars 50μm. (**D**) Representative immunoblot of RPA knockdown (siRPA) cells shown with transfection (siGAPDH) and gel loading (tubulin) controls. 25nM siRNA for 48h. MW in kDa left. (**E**) Cell-cycle phases in RPA knockdown or siGAPDH control (ctrl) cells. Coloured symbols indicate means from 3 biological replicate (60,000 cells per variable). Error bars SD. (**F**) Representative image of γH2AX RINGs (white arrow) in RPA knockdown cells. Scale bars 25μm. (**G**) Proportion of γH2AX RINGs in RPA knockdown cells -/+ toxin^{WT}. Non-transfected control (nt). Circles indicate means from fields of view in 2 biological replicates (122 nuclei per variable). Error bars SEM. (**H**) Representative immunoblot of super-RPA cells -/+ toxin^{WT} analysed with indicated antibodies. Hyper-phosphorylated RPA32 (red arrow), non-phosphorylated RPA32 (blue arrow). MW in kDa left. (**I**) Proportion of γH2AX RINGs in super-RPA cells -/+ toxin^{WT}. 2 biological replicates (2000 nuclei per variable). Error bars SEM. (**J**) Representative image of γH2AX in U2OS control cells (ctrl) or super RPA U2OS cells stably expressing recombinant RPA complex intoxicated with 5ng/ml toxin^{WT}. Scale bars 5μm. In representative images (**C, F, G**) outlines of DAPI-stained nuclei are shown. Statistical significance (**** = P<0.0001, *** = P<0.0002, ** = P<0.0021, * = P< 0.0332, ns = P>=0.05) was calculated between indicated experiments using an unpaired two-sided *t* test (**B**), or calculated relative to indicated controls using one-way ANOVA (**G, I**) or two-way ANOVA (**E**) together with a Tukey's multiple comparison test. Source data are provided as a Source Data file.

Figure 4. Typhoid toxin exhausts RPA by oversupply of ssDNA substrate.

(**A**) Representative image of toxin-induced RPA exhaustion. HT1080 cells intoxicated with toxin^{WT} or toxin^{HQ} for 2h before polymerisation of double-stranded BrdU-labelled DNA from sites of exposed ssDNA template at 24h (ssDNA, magenta). ssDNA-bound RPA32 pT21 (pRPA, cyan) shown with BrdU shown in grayscale for clarity (ssDNA foci). Insets of toxin^{WT} magnify ssDNA foci unprotected by pRPA (blue arrow) or partially protected by pRPA indicated by white co-localisation staining (white arrow). Insets of toxin^{HQ} show RPA-bound ssDNA. Scale bars 10μm. (**B**) Proportion of BrdU-labelled ssDNA foci per nucleus in intoxicated HT1080 cells. Aphidicolin (APH) was used as positive control for ssDNA induction and toxin^{HQ} used as a negative control. Coloured circles indicate means from fields of view. 2 biological replicates (160 nuclei per variable). Error bars SEM. (**C**) Proportion of serum-starved cells with RPA32 pT21 foci (pRPA). Coloured circles indicate means from technical replicates (2 biological replicates, 900 nuclei/variable). Error bars SEM. (**D**) Proportion of cells with RPA32 pT21 foci (pRPA) in presence of serum. Coloured circles indicate means from technical replicates (2 biological replicates, 900 nuclei/variable). Error bars SD. (**E**) Representative image of RPA32 pT21 (pRPA, grayscale) with γH2AX (magenta) RINGs (blue arrows) in cells treated with APH as indicated. Scale bars 50μm. (**F**) Proportion of γH2AX RINGs in APH-treated cells -/+ toxin^{WT} as indicated. Coloured circles indicate means from fields of view (2 biological replicates, 600 nuclei/variable). Error bars SEM. (**G**) Mean RPA pT21 (pRPA) foci intensity in APH-treated cells -/+ toxin^{WT} as indicated. Coloured circles indicate means from fields of view (2 biological replicates, 600 nuclei/variable). Error bars SEM. A.U, arbitrary units. In representative images (**A, E**) outlines of DAPI-stained nuclei are shown. Statistical significance (**** = P<0.0001, *** = P<0.0002, ** = P<0.0021, * = P< 0.0332, ns = P>=0.05) was calculated relative to toxin^{HQ} using one-way ANOVA and a Dunnett's multiple comparison test (**B**), or relative to untreated via one-way ANOVA and a Tukey's multiple comparison test (**C, D, F, G**). Source data provided as a Source Data file.

Figure 5. RING-induction by the toxin drives senescence and infection.

(**A**) Representative image of toxin-induced cell growth arrest and distension. HT1080s either untreated or treated with toxin^{WT} or toxin^{HQ} for 2h before imaging at 7-days. Cell colonies (top panel) and high-magnification images (bottom panel). Arrows mark individual cells. Scale bars 50μm. (**B**) Representative image of SA-β-Gal activity in intoxicated cells. Scale bars 50μm. (**C**) Proportion of intoxicated cells with SA-β-Gal activity relative to untreated. Analysed 1700 cells/variable, error bars SD. (**D**) Representative image of toxin-induced SA-β-Gal in γH2AX RING cells at 48h. Blue arrows indicate senescent RING cells (γH2AX in magenta/SPiDER β-Gal in grayscale) and distended nuclei (DAPI, grayscale). White arrows indicate non-senescent cells. Scale bars 50μm. Proportion of cells with SA-β-Gal activity following (**E**) intoxication with toxin^{WT} -/+

serum (350 cells/variable, error bars SD), (**F**) RPA knockdown (900 cells/variable, error bars SEM), (**G**) APH-treatment (900 cells/variable, error bars SD), and (**H)** infection with wild-type (*Sm*^{WT}) or toxin-deficient (*Sm*$^{\Delta cdtB}$) *S.*Javiana (3500 cells/variable, error bars SEM). (**I**) Experimental pipeline for J, K and L assaying toxin-induced transmissible senescence. Conditioned medium harvested from cells 24h post-treatment, as indicated, was incubated with fresh cells for 6-days before assaying: (**J**) SA-β-Gal activity in HT1080s (1240 cells/variable, error bars SD). (**K**) γH2AX (green) positive HT1080 cell nuclei (DAPI, blue). 1 biological replicate, 300 cells/variable, error bars SD. Representative γH2AX images shown left. Scale bars 50μm. (**L**) *Salmonella* infection of THP1s. 370 cells/variable, error bars SD. Representative images of THP1s (DAPI, blue) infected with *Salmonella*$^{\Delta cdtB}$ (green), left. Scale bars 50μm. In graphs, coloured circles indicate means from technical replicates (2 biological replicates, unless indicated otherwise). Statistical significance (**** = P<0.0001, *** = P<0.0002, ** = P<0.0021, * = P< 0.0332, ns = P>=0.05) was calculated relative to control (indicated by lack of p-value) using a one-way ANOVA and a Tukey's multiple comparison test (**C, G, J, K, L**), or an unpaired two-sided t test (**E, F, H**). Source data are provided as a Source Data file.

Figure 6. Proposed Model

Left: (A) Control cells undergo DNA replication where RPA protects ssDNA from breakage. (B) Cells divide, and (C) no senescence is observed, which impairs *Salmonella* infection.

Right: (D) The typhoid toxin causes an initial burst of DNA damage in G1 that combines with damage in S-phase to cause replication stress by oversupply of the RPA substrate ssDNA. (E) RPA sequestration causes DNA damage that manifests as γH2AX RINGs. (F) RING cells enter into a senescence-like state resulting in SASP-induced transmissible senescence that promotes *Salmonella* invasion into host cells. Thus, toxin manipulation of infection niches via senescence may contribute to chronic *Salmonella* infections, which are associated with the typhoid toxin[14, 16, 57].

Fig 1

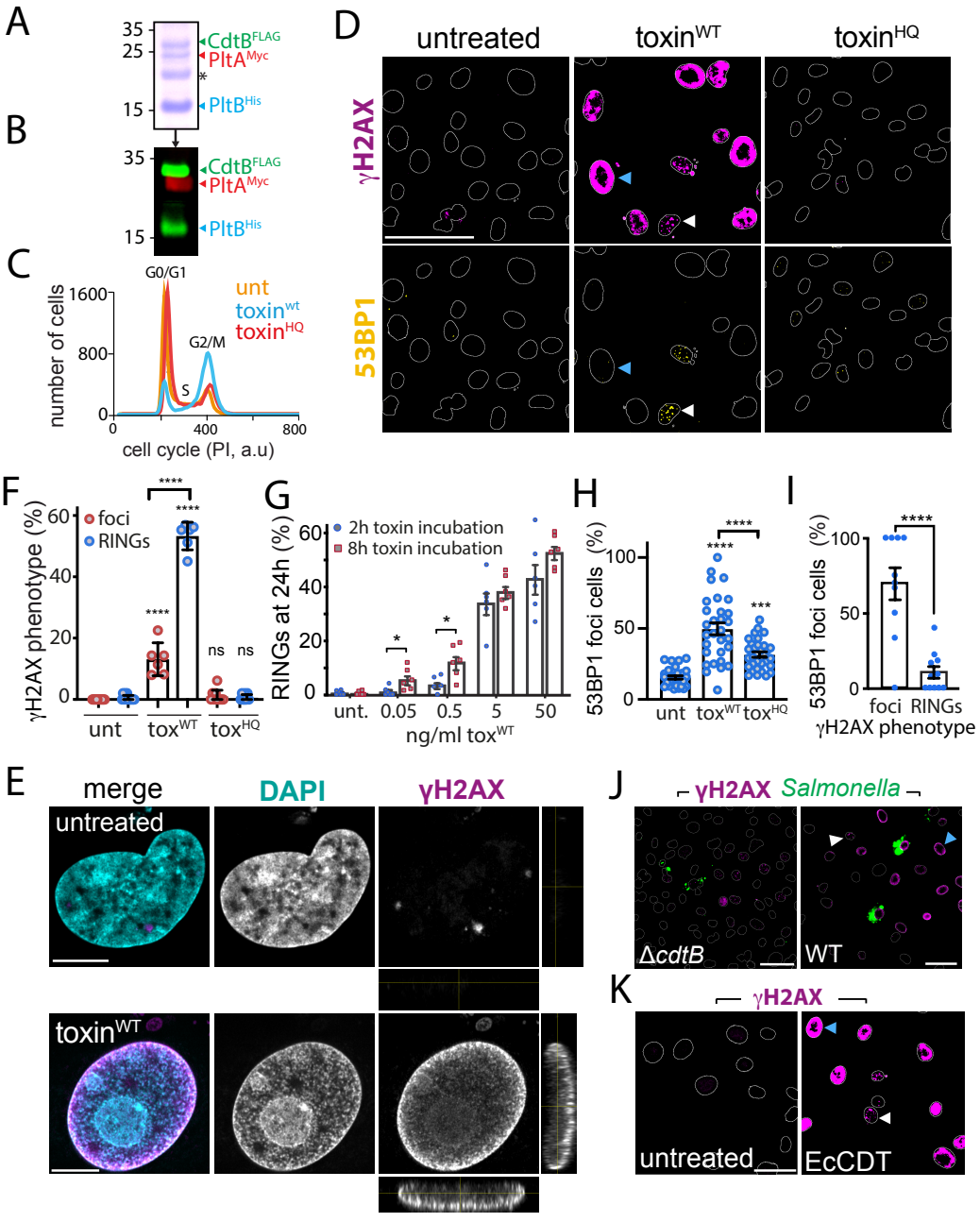
A
35
25
15
CdtB^FLAG
PltA^Myc
PltB^His
B
C
G0/G1
G2/M
S
unt
toxin^wt
toxin^HQ
number of cells
cell cycle (PI, a.u)
D
untreated
toxin^WT
toxin^HQ
γH2AX
53BP1
F
γH2AX phenotype (%)
foci
RINGs
unt
tox^WT
tox^HQ
ns
G
RINGs at 24h (%)
2h toxin incubation
8h toxin incubation
ng/ml tox^WT
H
53BP1 foci cells (%)
I
E
merge
DAPI
γH2AX
untreated
toxin^WT
J
γH2AX Salmonella
ΔcdtB
WT
K
EcCDT

Fig 2

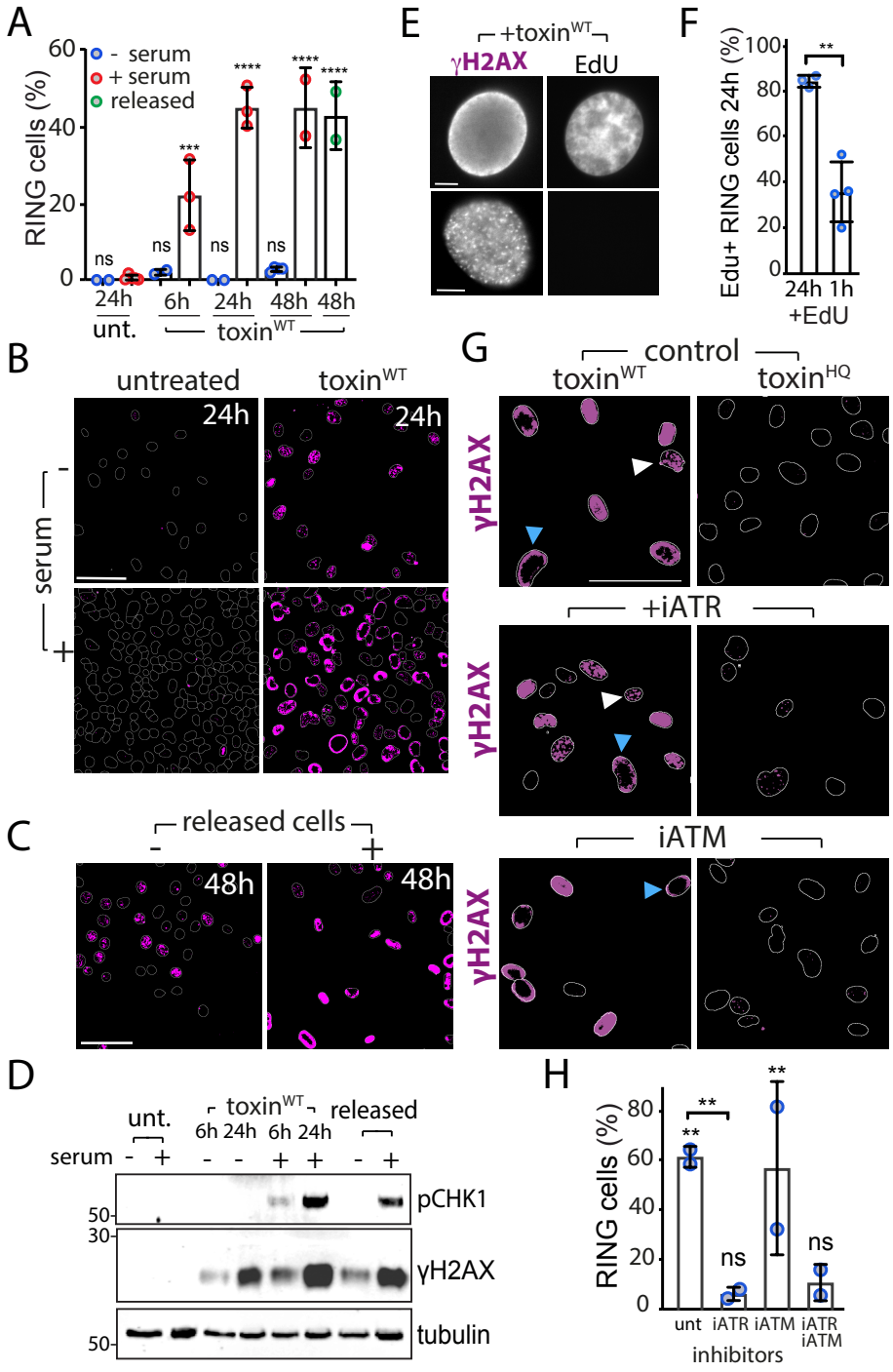
A
RING cells (%)
- serum
+ serum
released
ns
***
****
24h
6h
24h
48h
48h
unt.
toxin^WT
B
untreated
toxin^WT
24h
serum
C
released cells
48h
D
unt.
toxin^WT
released
6h 24h 6h 24h
serum
pCHK1
γH2AX
tubulin
E
+toxin^WT
γH2AX
EdU
F
Edu+ RING cells 24h (%)
24h 1h
+EdU
G
control
toxin^WT
toxin^HQ
γH2AX
+iATR
iATM
H
RING cells (%)
unt
iATR
iATM
iATR iATM
inhibitors

Fig 3

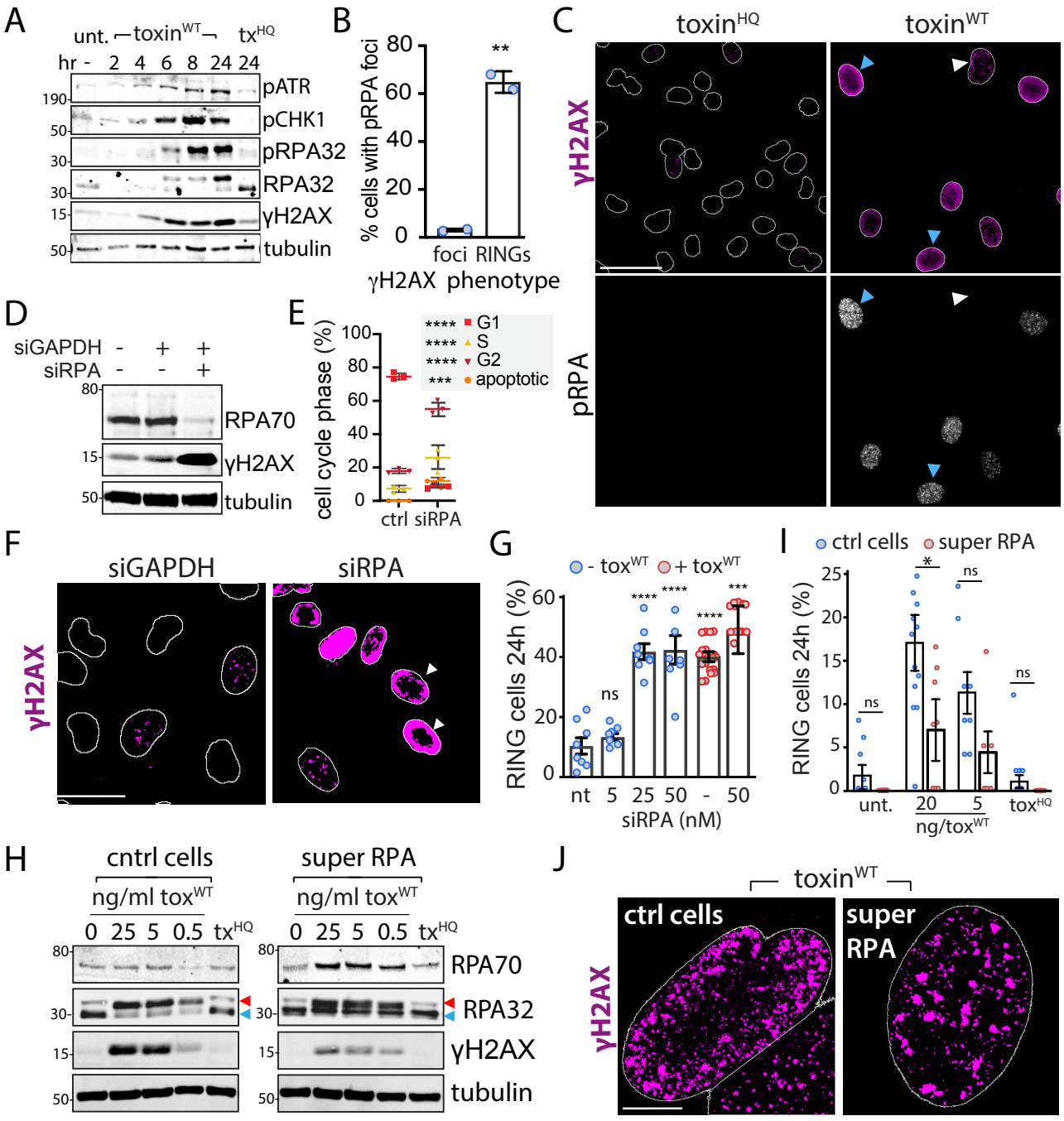
A
unt.
toxin^WT
tx^HQ
hr - 2 4 6 8 24 24
190
50
30
30
15
50
pATR
pCHK1
pRPA32
RPA32
γH2AX
tubulin
B
% cells with pRPA foci
80
60
40
20
0
**
foci RINGs
γH2AX phenotype
C
toxin^HQ
toxin^WT
γH2AX
pRPA
D
siGAPDH - + +
siRPA - - +
80
15
50
RPA70
γH2AX
tubulin
E
cell cycle phase (%)
100
80
60
40
20
0
**** G1
**** S
**** G2
*** apoptotic
ctrl siRPA
F
siGAPDH
siRPA
γH2AX
G
- tox^WT
+ tox^WT
RING cells 24h (%)
60
40
20
0
ns
****
****
****
***
nt 5 25 50 - 50
siRPA (nM)
I
ctrl cells
super RPA
RING cells 24h (%)
25
20
15
10
5
0
*
ns
ns
ns
ns
unt. 20 5 tox^HQ
ng/tox^WT
H
cntrl cells
super RPA
ng/ml tox^WT
ng/ml tox^WT
0 25 5 0.5 tx^HQ
0 25 5 0.5 tx^HQ
80
30
15
50
80
30
15
50
RPA70
RPA32
γH2AX
tubulin
J
toxin^WT
ctrl cells
super RPA
γH2AX

Fig 4

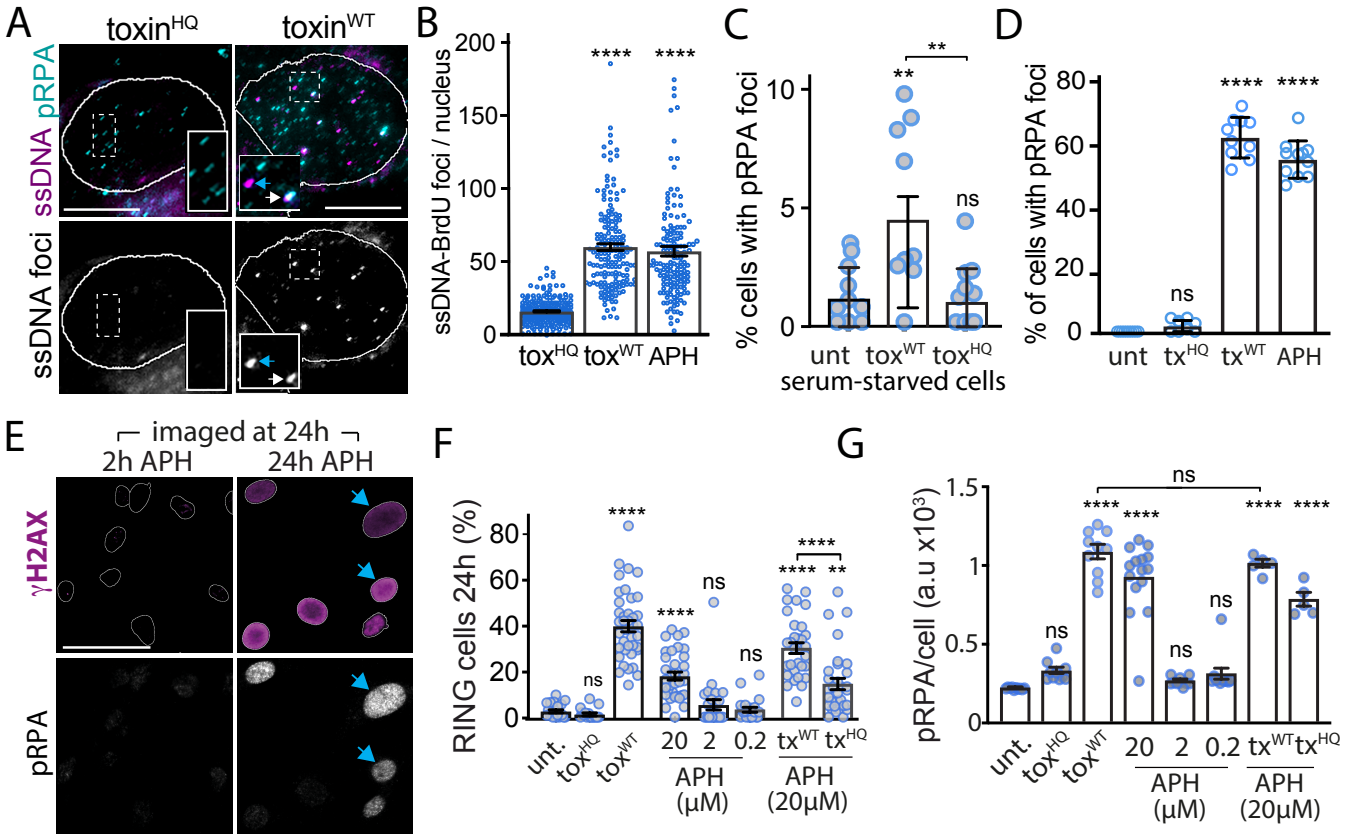
A
toxin^HQ
toxin^WT
ssDNA pRPA
ssDNA foci
B
ssDNA-BrdU foci / nucleus
tox^HQ tox^WT APH
C
% cells with pRPA foci
unt tox^WT tox^HQ
serum-starved cells
D
% of cells with pRPA foci
unt tx^HQ tx^WT APH
E
imaged at 24h
2h APH
24h APH
γH2AX
pRPA
F
RING cells 24h (%)
unt. tox^HQ tox^WT
20 2 0.2 tx^WT tx^HQ
APH (μM)
APH (20μM)
G
pRPA/cell (a.u x10^3)
unt. tox^HQ tox^WT
20 2 0.2 tx^WT tx^HQ
APH (μM)
APH (20μM)

Fig 5

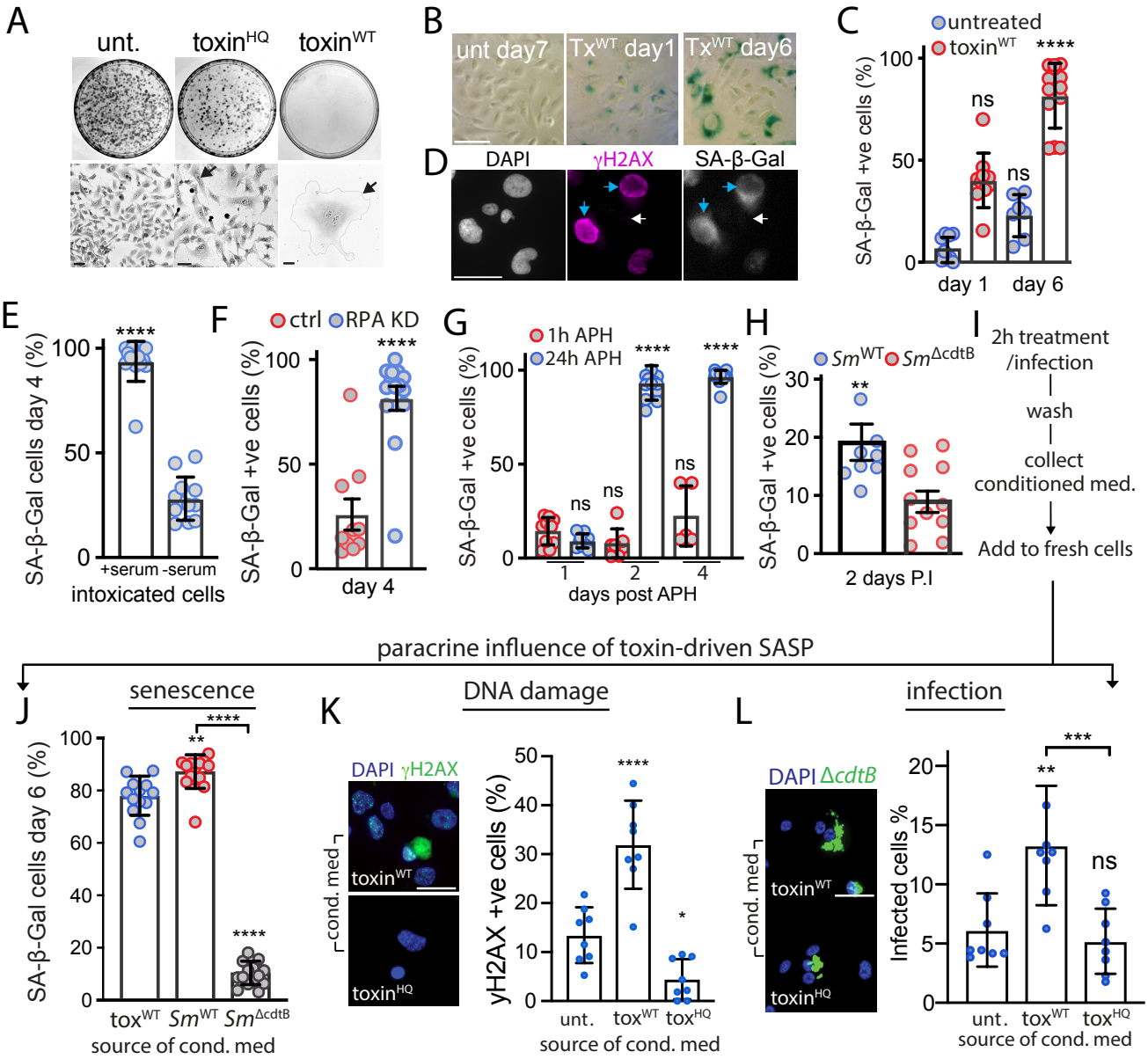
A
unt.
toxin^HQ
toxin^WT
B
unt day7
Tx^WT day1
Tx^WT day6
C
untreated
toxin^WT
SA-β-Gal +ve cells (%)
ns
ns
****
day 1
day 6
D
DAPI
γH2AX
SA-β-Gal
E
SA-β-Gal cells day 4 (%)
****
+serum
-serum
intoxicated cells
F
ctrl
RPA KD
SA-β-Gal +ve cells (%)
****
day 4
G
1h APH
24h APH
SA-β-Gal +ve cells (%)
ns
ns
ns
****
****
days post APH
H
Sm^WT
Sm^ΔcdtB
SA-β-Gal +ve cells (%)
**
2 days P.I
I
2h treatment /infection
wash
collect conditioned med.
Add to fresh cells
paracrine influence of toxin-driven SASP
J
senescence
SA-β-Gal cells day 6 (%)
**
****
****
tox^WT
Sm^WT
Sm^ΔcdtB
source of cond. med
K
DNA damage
DAPI γH2AX
cond. med
toxin^WT
toxin^HQ
γH2AX +ve cells (%)
****
*
unt.
tox^WT
tox^HQ
source of cond. med
L
infection
DAPI ΔcdtB
cond. med
toxin^WT
toxin^HQ
Infected cells %
**
***
ns
unt.
tox^WT
tox^HQ
source of cond. med

Fig 6

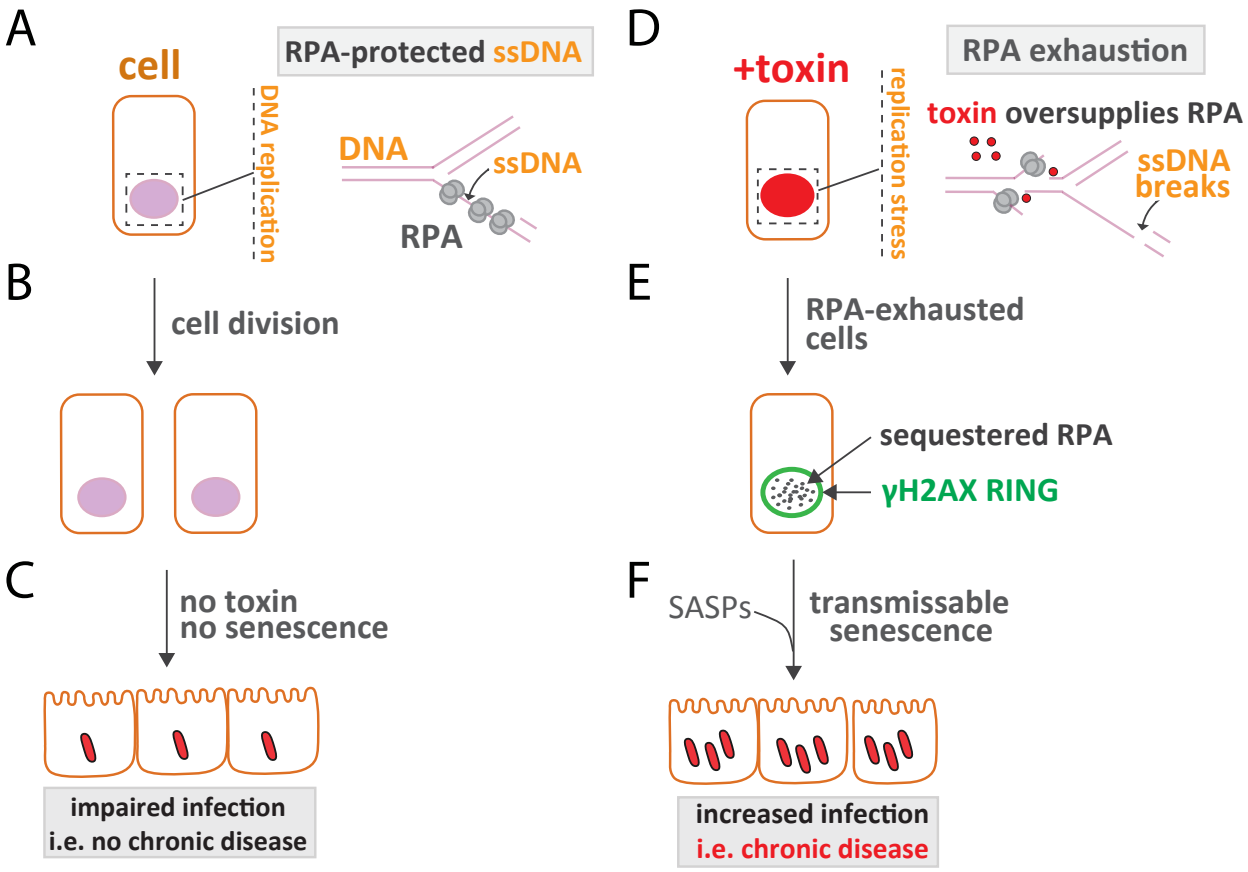
A
cell
RPA-protected ssDNA
DNA replication
DNA
ssDNA
RPA
B
cell division
C
no toxin
no senescence
impaired infection
i.e. no chronic disease
D
+toxin
RPA exhaustion
replication stress
toxin oversupplies RPA
ssDNA
breaks
E
RPA-exhausted
cells
sequestered RPA
γH2AX RING
F
SASPs
transmissable
senescence
increased infection
i.e. chronic disease